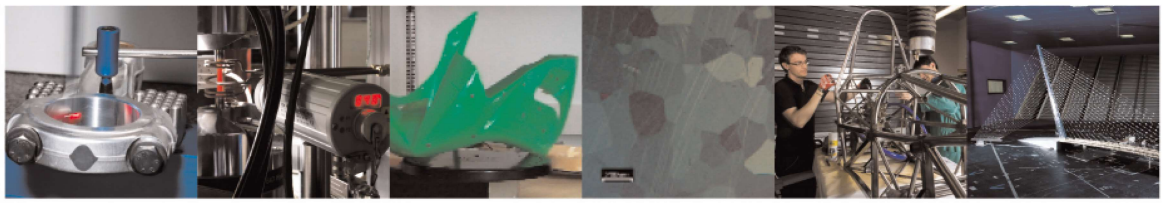

# Multi-robot spot-welding cells for car-body assembly: Design and motion planning

Pellegrinelli, Stefania; Pedrocchi, Nicola; Tosatti, Lorenzo Molinari; Fischer, Anath; Tolio, Tullio

This is a post-peer-review, pre-copyedit version of an article published in ROBOTICS AND COMPUTER-INTEGRATED MANUFACTURING. The final authenticated version is available online at: http://dx.doi.org/10.1016/j.rcim.2016.08.006



DIPARTIMENTO DI MECCANICA ■ POLITECNICO DI MILANO
via G. La Masa, 1 ■ 20156 Milano ■ EMAIL (PEC): pecmecc@cert.polimi.it
http://www.mecc.polimi.it
Rev. 0

# Multi-robot spot-welding cells for car-body assembly: Design and motion planning

Stefania Pellegrinelli [a,b,c,*], Nicola Pedrocchi [a], Lorenzo Molinari Tosatti [a], Anath Fischer [c], Tullio Tolio [a,b]

[a] Institute of Industrial Technologies and Automation (ITIA), National Research Council of Italy (CNR), Milano, Italy
[b] Department of Mechanical Engineering, Politecnico di Milano, Milano, Italy
[c] Faculty of Mechanical Engineering, Technion, Haifa, Israel

A B S T R A C T

Multi-robot cells for spot welding use coordinated robots to assemble metal panels via spot welding by coordinated robots, for instance in the construction of car doors. The design of multi-robot cells for spot welding required both cell design and off-line motion planning. Cell design involves resource selection (such as robots and welding guns) and resource configuration, while considering cell productivity, costs, flexibility and reconfigurability. Motion planning involves allocating welding points to each resource and calculating collision-free motion plan for each robot. Currently, cell design and motion planning are sequential and manual activities, managed by different and separate industrial functional units. This results in several cycles before the design converges to a feasible final solution. The proposed approach introduces a unified methodology, aiming at optimizing the holistic cell design and motion planning, that reduces design time and errors. The feasibility of the proposed approach has been demonstrated in several ad-hoc basic replicable cases and in one industrial case. The outcome of this research improves state of the art, reducing design and motion planning time over current technology. Moreover, the method has been integrated into a computerized approach which has the potential to accelerate the whole cell design and motion planning processes and to reduce human efforts.

*Keywords:*
Multi-robot cell
Motion planning
Cell design
Robot coordination

## 1. Introduction

Over the past 20 years, the automotive industry has moved towards the assembly of different vehicle models on the same assembly line through flexible and reconfigurable multi-robot cells [1,2]. This shift reflects two major drivers in automotive production: the saturation of the production capacity to reduce the production costs; the increase of product flexibility in terms of new vehicle models, and customization [3,4].[1]

Vehicle body-in-white is obtained through the assembly of ~300 – 500 metal panels and sheet components. These panels, produced through different processes such as stamping and machining, are generally provided in 'white', i.e., unprimed and unpainted. They are assembled into sub-assemblies necessary for the definition of the vehicle upper body or lower body, e.g., front and rear doors, front and rear trails, and the body-in-white, i.e., the assembly of the upper and lower body. The assembly of metal panels and sub-assemblies requires dedicated lines. The number of multi-robot welding cells can vary among the lines (generally between 55 and 75 cells per line) and depends on the total number of needed welding points, possible precedence constraints in the execution sequence of the welding points and in the desired takt time (average unit production time needed to meet customer demand) [6]. Each spot-welding assembly cell is an environment constituted, as in depicted in Fig. 1, by body-in-white transportation device so that the body-in-white can enter and exit the cell; body-in-white fixture to hold the body-in-white during the welding process; industrial robots; welding guns to be mounted on the robots; robot support structure to fix the robot in the space. The robot support structure influences the possible robot position and orientation in the cells. These selectable devices determine the cell cycle time that has to be minor or equal to the line takt time.

In the current industrial practice, automotive companies, proving all the necessary specifications such as the required cycle time (RCT) and consequently the talk time, commission turnkey systems to original equipment manufacturers (OEMs) that act as

* Corresponding author at: Institute of Industrial Technologies and Automation (ITIA), National Research Council of Italy (CNR), Milano, Italy.
*E-mail address:* stefania.pellegrinelli@itia.cnr.it (S. Pellegrinelli).

[1] In US, the number of vehicle models doubled from 1980 to 1999 (1050 models in 2000); in China, the number of vehicle models increased from 278 in 2010 to 474 in 2014 [5].

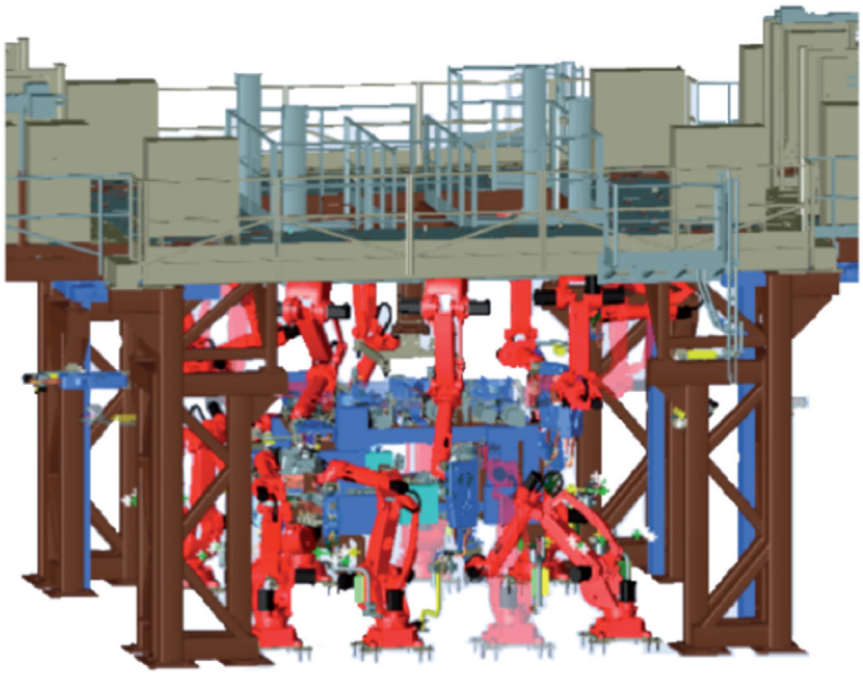

**Fig. 1.** Multi-robot spot-welding cell - COMAU Robogate. Courtesy of COMAU Robotics™.

system integrators. On the basis of the received specifications, the OEM initially solves the multi-robot cell design problem and subsequently provides a feasible robot motion plan, making cell design and motion planning two sequential activities generally managed from different industrial functional units. Firstly, taking into account position of welding points required by the automotive company, the OEM designs the body-in-white fixture (*BF*) that will influence the final quality of the body-in-white and the transportation device (*BTD*). Secondly, the OEM preliminary selects the resources in term of "which", "where", "how many" robots and tools are needed. Specifically, they select the robot model (*RM*), the robot support structure model (*RSM*), the robot positions and orientations (*RPOs*) on the robot support structure, and a welding gun model (*WGM*) for each robot in the cell. This activity is mainly based on tabular information coming from the OEM's experience and expertize. Finally, the OEM allocates the welding points to the robots, defines a motion plan for each robot and solves coordination issues among the robots. However, the mutual-influence of the multi-robot cell design and motion planning cannot be ignored: the decoupling of design and planning activities could lead to infeasible motion plans, imposing changes to the cell design. Thus, mutual interactions and cycles could be needed to obtain a feasible final solution. Each cycle causes delays and accumulated errors in a process that generally requires up to 14 weeks of works. This separation of the activities is partially justified by (i) the complexity of the two steps that represents a barrier for a straightforward optimal solution, and (ii) the multi-disciplinary activities and research fields required. The separation of multi-robot cell design and off-line motion planning that characterizes the industrial practice can also be identified in literature, where the integration between the two activities has not been adequately investigated so far.

## 2. Overview

This section focuses on the state of the art with respect to the following topics: design of multi-robot systems with a focus on multi-robots in assembly spot-welding cells; robot motion planning; and simultaneous design and motion planning of robotic cells. The innovative aspects of the proposed approach will be compared to these state of the art methods in Section 3.

### 2.1. Multi-robot cell design for spot-welding assembly

Several papers deal with the problem of designing spot welding cells, where each paper focuses only on partial aspects of the problem. A computer-aided process planning (CAPP) platform for integrating robot systems in small and medium enterprises is presented in [7]. However, the paper only defines the framework for cell design without addressing problems related to the design process.

On the contrary, an approach to optimally identify the gun model and the robot installation position for a single robot is described in [8], taking into account the flexibility of the production system and the versatility of the equipment. A similar approach is introduced by [9], where a single robot is optimally placed in order to execute some predefined tasks. Task reachability is checked for several possible discrete positions of the robot, taking into account collisions with objects in the environment. Other approaches focusing on the optimization of the robot position in the cell or the robot selection are described in [10,11].

Michalos et al. [12] marks a step forward in the state of the art, analyzing the design of multi-robot cells. Specifically, the paper proposes a more comprehensive approach for the design of multi-robot assembly cells to derive assembly line design alternatives. Given the product specifications and a set of possible technologies, layouts, resources and operations, alternative solutions are generated. Investment costs, cell availability, resource reutilization, flexibility and mean annual production volume are calculated for each solution. Although the presented methodology was applied to an automotive case, the allocation of the tasks to the robots is not considered for optimization.

The problem of the production tooling structure for multi-robot spot-welding assembly cells is considered in [13–16]. This approach focuses on the identification of the flexible elements of vehicle body-in-white and their interaction with the production tooling structure. The aim is to provide a reconfigurable and

flexible production tooling structure, so that body-in-white styling changes and variants can be easily produced without the need of tooling changeover.

### 2.2. Off-line motion planning for multi-robot cells

Off-line motion planning for multi-robot cells concerns with the automatic generation of collision-free coordinated trajectories. Each robot has to move from a starting position to a goal position avoiding environmental obstacles and other robots.

Motion planning problem for a single robot has been widely discussed in literature [17]. The most common techniques are: potential fields, roadmaps, cell decomposition, probabilistic potential fields, probabilistic roadmaps, probabilistic cell decomposition and simple-query sampling-based method. The efficiency and efficacy of these techniques are problem dependent. The problem of robot motion is traditionally based on decoupled and centralized approaches.

Decoupled planning defines the motion of each robot individually, where in the first phase, the existence of other robots is ignored; then, in the second phase, the resulting paths are combined by resolving possible collisions between the paths through velocity tuning [18,19] or path modification [20]. Such algorithms search smaller-dimensional spaces but there is no guarantee for finding an existing solution.

Centralized motion planning considers a set of robots, operating in the same workspace as a single multi-body robot. The main problem related is the high dimensionality of the configuration space. A coordinated motion planning approach based on probabilistic roadmaps (PRMs), which is probabilistically complete, is proposed in [21]. Another method [22,23] is demonstrated on a simulated six-robot welding station combining 36 degrees of freedom. It shows that centralized planning based on PRM and lazy collision has been a much more effective approach than decoupled planning.

### 2.3. Cell design and motion planning

Few researches have investigated the influence of cell design on motion planning, and almost all of them have focused on some relations among set of factors in the design and motion planning areas and in simplified environments.

Some approaches face the design and the motion planning in two separate steps. In [24], a 3D optimized layout for assembly cells is proposed when resources, tasks and product geometry are given. The components are roughly placed in the environment in order to generate a starting solution. Then, their position is optimized to guarantee the accessibility of all required locations. Once cell design is given, a path planning is generated. Similarly, in [25], conveyor belt and robot positions are optimized through a simulation-based approach. Once a possible layout is generated, robot trajectories are calculated taking into account the pre-allocated and predefined tasks.

Design and motion planning integration is presented in [26–28]. In [26], the most appropriate manipulator systems are selected from a set of candidates, while optimizing their location and their motion coordination. Even if the simultaneous resolution of design and motion coordination is addressed, design only copes with robot selection and placement, thus disregarding end effector selection and task allocation. An extended approach for the design of a cooperating robot cell is described in [27,28]. Starting from an initial rough solution, a final collision-free solution with optimized cycle time is found. However, limitations exist in relation to the motion planning coordination activities, where only the collisions between the robot end effector, the floor and the part are considered.

A large amount of simulation software tools are available for robot systems such as CimStation [29], Robcad [30], RobotStudio [31], 3DAutomate [32], Delmia [33] and Industrial Path Planner [34]. These software tools cover one or more tasks in robotics like off-line programming, design of robot work cells, collision detection, trajectory optimization and so on. However, none of them is able to solve all these problems simultaneously, thus selecting the required resources, defining the resource layout and providing a motion plan at the same time.

At the best of the author knowledge, therefore, the state-of-the-art approaches and software tools cope only with some different problems related to the design and motion planning, under several hypotheses that highly limit the applicability field. Furthermore, the interdependence between design and motion planning is only partially addressed in the state of the art.

### 2.4. Research contribution and objectives

The proposed method simultaneously handles cell design and motion planning problems. The contribution of this paper is to demonstrate the feasibility and advantages of integrating multi-robot spot-welding cell design and motion planning in real industrial contexts. The research contributes to the area as follows:

- Provides a formalization of the design and motion planning problem for multi-robot spot-welding cells by considering both industrial practice and state of the art methods.
- Analyzes the influence of the cell design step on motion planning, and vice versa.
- Creates a simultaneous resolution of the cell design and motion planning.
- Develops a decoupled motion planning technique for high-dimensional $\mathcal{C}$-spaces with ad-hoc algorithms for multi-robot spot-welding cells.
- Tests main motion planning techniques in an environment with high complexity [17].

Moreover, the research contributes to the industrial practice as follows:

- Minimizes time delays of the overall activity.
- Creates solutions that are robust to accumulated errors.
- Provides computerized solutions that are independent from the worker's skills, and reduce drastically his/her effort.

## 3. The methodology

The proposed method is based on a set of formalized inputs and outputs that reflects the industrial practice. The set of inputs is related to the specifications provided by the automotive company (Table 1) and to the resources that the OEM can consider for the cell design (Table 2), i.e. robot model, robot support structure, robot positions and orientations on the robot support structure and welding gun models. On the basis of this set of inputs, the method identifies as outputs both the cell design and the motion planning, granting the minimum of the total investment cost (Table 3).

The approach, representing a novelty in the state-of-the-art, consists of four stages (Fig. 2):

– *Stage 1* – Single-robot off-line motion planning;
– *Stage 2* – Off-line collision check of two robot paths;
– *Stage 3* – Multi-robot cell design and off-line motion planning;
– *Stage 4* – Motion plan validation.

**Table 1**
Automotive company's inputs.

| | |
|---|---|
| ***CBS*** (and/or ***BIW***) | Metal sheets that have to be assembled for the creation of the car body (Car Body metal Sheets and/or Body In White); CAD file is required as well as its orientation and position in the cell. |
| ***WPs*** | $\{WP_{wp}: wp=0,\ldots, N^{WP}-1\}$ Welding Points (depending on *CBS*) expressed as position [mm] and Euler ZYZ rotation [°] respect to the cell reference system together with a rotation range that represent the possible rotations of the gun around its Z axis during welding process; $N^{WP}$ denotes the number of *WPs*. |
| ***BF*** | Fixtures for the blocking of the metal sheets during the welding process (car Body Fixture); designed by the OEM but approved by the automotive company; CAD file is required as well as its orientation and position in the cell. |
| ***BTD*** | Device to allow the transportation of the car body into the cell (Body Transportation device); CAD file is required as well as its orientation and position in the cell. |
| $WT_{wp}$ | Welding Time for the welding point $wp$–th. |
| ***RCT*** | Maximum allowed cycle time for the assembly process (Required Cycle Time). |

**Table 2**
OEM's inputs.

| | |
|---|---|
| ***RM*** | Robot Model. The method considers only one robot model per cell according to the industrial practice and for sake of clarity. The relaxation of this hypothesis will lead to the increase in the problem complexity; CAD file and D&H parameters are required for each robot model. |
| ***RPOs*** | $\left\{ RPO_{rpo}: rpo=1,\ldots, N^{RPO} \right\}$, set of possible positions and orientations of the robot in the cell; $N^{RPO}$ denotes the maximum number of possible *RPOs*; |
| ***RSM*** | Model of support structure on which the robot are mounted (Robot Support structure Model) leading to the definition of *RPOs*; the CAD file is required. |
| ***WGMs*** | $\left\{ WGM_{wgm}: wgm=1,\ldots, N^{WGM} \right\}$,set of welding gun models (Each robot may be provided with a different $WGM_{wgm}$); $N^{RPO}$ denotes the number of possible welding gun models; CAD file is required as well as the rototranslation matrices describing the position of the gun control point in the gun system and the gun system in the tool robot reference system. |
| $NC^{RM}$, $NC^{RSM}$, $NC^{WGM_{wgm}}$ | Number of already aCquired resources, i.e. resources that are already available and do not have to be acquired. Specifically: number of available robots for each *RM* (Number of aCquired Robot Models), availability of the *RSM* (Number of aCquired Robot support Structures), number of available welding guns for each $WGM_{wgm}$ (Number of aCquired Welding Gun Models). |
| $COST^{RM}$, $COST^{RSM}$, $COST^{WGM}$ | Cost per unit of *RM* [€], cost of the *RSM* [€] on which the robot are mounted, cost per unit of $WGM_{wgm}$ [€]. |

**Table 3**
*Outputs*.

| | |
|---|---|
| ***COST*** | Investment COST of the cell [€], i.e. costs related to the resources to be acquired (robot, welding guns and robot support structure) |
| $TN^{RM}$ | Total Number of selected robots for the considered *RM* in the welding cell; |
| $TN^{WGM_{wgm}}$ | Total Number of selected welding guns for each *WGM*. |
| $RGP_{wgm,rpo}$ | Allocation of the welding gun model to each robot position and orientation – Binary variable equal to 1 if robot mounting $WGM_{wgm}$ is in position/orientation $RPO_{rpo}$. |
| $WPA_{rpo,wp}$ | allocation of the welding point $WP_{wp}$ to the robot $RPO_{rpo}$ - binary variable equal to 1 if the welding point $WP_{wp}$ is allocated to $RPO_{rpo}$. |
| $I^{wgm,rpo}_{wp_1,wp_2}$ | Starting time of the trajectory that allows robot in $RPO_{rpo}$ mounting $WGM_{wgm}$ to move from $WP_{wp_1}$ to $WP_{wp_2}$ and weld $WP_{wp_2}$ [s]. |
| $C^{wgm,rpo}_{wp_1,wp_2}$ | completion time of the trajectory that allows robot in $RPO_{rpo}$ mounting $WGM_{wgm}$ to move from $WP_{wp_1}$ to $WP_{wp_2}$ and weld $WP_{wp_2}$ [s]. |
| $OCT_{rpo}$ | Obtained Cycle Time for robot in $RPO_{rpo}$ [s] - time required by the robot in $RPO_{rpo}$ to weld all the allocated WPs and be back to the initial configuration |
| ***MAXOCT*** | Obtained Cycle Time for cell design [s] - time required by all robots to weld the allocated WPs and be back to initial configuration. |
| $MP^{wgm,rpo}_{wp_1,wp_2}$ | Binary variable equal to 1 if robot in $RPO_{rpo}$ mounting $WGM_{wgm}$ processes $WP_{wp_2}$ immediately after the $WP_{wp_1}$- it describes the final motion plan for the cell. |

Stage 1 first identifies all the possible single-robot systems derived by the available combinations of robot model, robot position and orientation on the robot support structure and welding guns. Then, it generates a set of collision-free trajectories (off-line motion plans) for each single-robot system exploiting the main principle of probabilistic roadmaps. Specifically, for each single-robot system, the algorithm defines collision-free trajectories among all the possible couples of reachable welding points. Thus, the outcome of this step is the mapping of the global solution space in terms of available possible motion plans per each possible input combination. Worthily, for each single-robot systems, a number of different motion plans is made available, since different welding points could be reached and the sequence is still not defined.

Stage 2, then, is a feasibility filter for the motion plans generated in Stage 1: for each couple of possible single-robot systems, the Stage evaluates if there are collisions (independently from the time coordinate) among the set of all the possible combination of motion plans. The Stage classifies two trajectories as safe or not safe. Two trajectories are safe when they do not collide whichever their starting time is. On the contrary, if two trajectories are classified as unsafe, they may collide and, therefore, their simultaneous execution is not allowed. Actually, the collision of two unsafe trajectories is not obvious: one or more combinations of their starting time may lead to a non-colliding execution. The choice not to simultaneously execute unsafe trajectories may lead to suboptimal motion plans.

Once defined the collision-free motion plans for all the single-robot systems, Stage 3 proposes an algorithm for the identification of the optimal multi-robot cell design in term of cell investment costs, i.e. the solution presents the minimum number of resources (robot, welding gun) to be acquired. Thus, the result is a complete cell design and a coordinated motion plan: the specification of each single-robot systems, the number of single-robot systems, and the sequence of welding points associated to each single-robot systems. Worthily, Stage 3 introduces in the optimization calculus

**Table 4**
Linear mixed-integer model for the optimal design of the multi-robot cell (Stage 3).

| | |
|---|---|
| **Resource data** | |
| $RM$ | See Table 2 |
| $RSM$ | See Table 2 |
| $RPO_{rpo}$ | See Table 2 |
| $WGM_{wgm}$ | See Table 2 |
| **Process related data** | |
| $WP_{wp}$ | See Table 1 |
| $RMP_{rmp}$ | $\{RMP_{rmp}: rmp=0, \ldots, N^{RMP}-1\}$, set of possible Robot Motion Plans; each motion plan is characterized by four indexes$\{wgm, rpo, wp_1, wp_2\}$ that refer to the welding gun $WGM_{wgm}$, the robot position and orientation $RPO_{rpo}$ and the welding points $WP_{wp_1}$, $WP_{wp_2}$; $N^{RMP}$ indicates all the existent $RMP(s)$. |
| $MPf^{wgm,rpo}_{wp_1,wp_2}$ | Binary variable equal to 1 if robot in $RPO_{rpo}$ mounting $WGM_{wgm}$ can process $WP_{wp_2}$ immediately after the $WP_{wp_1}$; 0 otherwise |
| $MT^{wgm,rpo}_{wp_1,wp_2}$ | Motion Time according to $MPf^{wgm,rpo}_{wp_1,wp_2}$ [s] - time required by the robot in $RPO_{rpo}$ to move from $WP_{wp_1}$ to $WP_{wp_2}$ and to execute $WP_{wp_2}$ |
| $WT_{wp}$ | Welding Time for $WP_{wp}$ ($WT_0$=0) [s] - time required to weld the considered welding point |
| $RCT$ | Required Cycle Time [s] - cycle time defined by the automotive company in order to cope with the expected throughput |
| $RWP$ | Number of times the robot initial points are replicated as waiting points |
| $IGP_{rpo_1,rpo_2}$ | binary variable equal to 1 if the robot in $RPO_{rpo_1}$ and the robot in $RPO_{rpo_2}$ display the same position and a different orientation; otherwise 0. This variable is useful in order to avoid the selection of more than one robot in each available position |
| $SP_{rpm_1,rpm_2}$ | Binary variable indicating a Safe couple of existing Plans - Equal to 1 (a) if robot in $RPO_{rpo}{}^{rpm_1}$ mounting $WGM_{wgm}{}^{rpm_1}$ and moving from $WP_{wp_1}{}^{rpm_1}$ to $WP_{wp_2}{}^{rpm_1}$ does not collide independently from the time coordinate with the robot in $RPO_{rpo}{}^{rpm_2}$ mounting $WGM_{wgm}{}^{rpm_2}$ and moving from $WP_{wp_1}{}^{rpm_2}$ to $WP_{wp_2}{}^{rpm_2}$ or (b) if robot in $RPO_{rpo}{}^{rpm_1}$ and robot in $RPO_{rpo}{}^{rpm_2}$ physically occupy the same position (independently from the orientation); otherwise 0 |
| $UP_{rpm_1,rpm_2}$ | Binary variable indicating an Unsafe couple of existing Plans - Equal to 1 if robot in $RPO_{rpo}{}^{rpm_1}$ mounting $WGM_{wgm}{}^{rpm_1}$ and moving from $WP_{wp_1}{}^{rpm_1}$ to $WP_{wp_2}{}^{rpm_1}$ could collide with the robot in $RPO_{rpo}{}^{rpm_2}$ mounting $WGM_{wgm}{}^{rpm_2}$ and moving from $WP_{wp_1}{}^{rpm_2}$ to $WP_{wp_2}{}^{rpm_2}$; otherwise 0 |
| **Resource related data** | |
| $NC^{RM}$ | See Table 2 |
| $NC^{WGM_{wgm}}$ | See Table 2 |
| $NC^{RSM}$ | See Table 2 |
| $COST^{RM}$ | See Table 2 |
| $COST^{WGM_{wgm}}$ | See Table 2 |
| $COST^{RSM}$ | See Table 2 |
| **Model data** | |
| $L$ | Value constant equal to 0.001 |
| **Process related decision variables** | |
| $MP^{wgm,rpo}_{wp_1,wp_2}$ | See Table 3 |
| $MPS^{wgm,rpo}_{wp_1,wp_2}$ | Binary variable equal to $k$ if robot in $RPO_{rpo}$ mounting $WGM_{wgm}$ processes $WP_{wp_2}$ immediately after the $WP_{wp_1}$ as $kth$ points. It describes the execution sequence of the $WPs$ for each robot/welding guns. |
| $MTT^{wgm,rpo}_{wp_1,wp_2}$ | Duration indicating the time required by robot in $RPO_{rpo}$ mounting $WGM_{wgm}$ to move from $WP_{wp_1}$ to $WP_{wp_2}$ and to weld $WP_{wp_2}$ [s] |
| $C^{wgm,rpo}_{wp_1,wp_2}$ | See Table 3 |
| $I^{wgm,rpo}_{wp_1,wp_2}$ | See Table 3 |
| $D^{wgm,rpo}_{wp_1,wp_2}$ | Temporal Delay for robot in $RPO_{rpo}$ mounting $WGM_{wgm}$ to move from $WP_{wp_1}$ to $WP_{wp_2}$ and weld $WP_{wp_2}$ after $WP_{wp_2}$ welding [s] |
| $WPA_{rpo,wp}$ | See Table 3 |
| $OCT_{rpo}$ | See Table 3 |
| $MAXOCT$ | See Table 3 |
| $TP_{rpm_1,rpm_2} \in \{0, 1\}$ | Binary variable equal to 1 if completion time of motion plans $RMP_{rpm_1}$ is minor than initial time of $RMP_{rpm_2}$, i.e. the trajectory of robot in $RPO_{rpo}{}^{rpm_1}$ mounting $WGM_{wgm}{}^{rpm_1}$ and moving from $WP_{wp_1}{}^{rpm_1}$ to $WP_{wp_2}{}^{rpm_1}$ is completed before the trajectory of the robot in $RPO_{rpo}{}^{rpm_2}$ mounting $WGM_{wgm}{}^{rpm_2}$ and moving from $WP_{wp_1}{}^{rpm_2}$ to $WP_{wp_2}{}^{rpm_2}$ starts; otherwise 0 |
| $SOP_{rpm_1,rpm_2}$ | Binary variable equal to 1 if motion plans $RMP_{rpm_1}$ and $RMP_{rpm_2}$ presents a temporal overlapping and are selected, i.e. robot in $RPO_{rpo}{}^{rpm_1}$ mounting $WGM_{wgm}{}^{rpm_1}$ and moving from $WP_{wp_1}{}^{rpm_1}$ to $WP_{wp_2}{}^{rpm_1}$ has a trajectory that temporally overlaps the trajectory of the robot in $RPO_{rpo}{}^{rpm_2}$ mounting $WGM_{wgm}{}^{rpm_2}$ and moving from $WP_{wp_1}{}^{rpm_2}$ to $WP_{wp_2}{}^{rpm_2}$; otherwise 0 |
| $ISP_{rpm_1,rpm_2}$ | Auxiliary variable used for the definition of $SOP_{rpm_1,rpm_2}$ |
| **Resource related decision variables** | |
| $COST$ | See Table 3 |
| $TN^{RM}$ | See Table 3 |
| $TN^{WGM_{wgm}}$ | See Table 3 |
| $NA^{RM}$ | Number of $RM$ to be Acquired |
| $NA^{WGM_{wgm}}$ | Number of Welding Guns to be Acquired for each $WGM$ |
| $NA^{RSM}$ | Number of $RSM$ to be Acquired |
| $TN^{RM'}$ | Support variable for the definition of $TN^{RM}$ |
| $TN^{WGM'_{wgm}}$ | Support variable for the definition of $TN^{WGM_{wgm}}$ |
| $RGP_{wgm,rpo}$ | See Table 3 |

**Table 5**
Simplified case – resource costs.

| Cost [€] | Value |
|---|---|
| $COST^{RM}$ | 24000 |
| $COST^{RSM}$ | 230000 |
| $COST^{WGM_{wgm}}$ | 9000 8500 |

**Table 6**
Simplified case 1 – solution.

| $RPO$ | $WGM$ | $WP$ seq. | $OCT_{rpo}$ [s] |
|---|---|---|---|
| $RPO_1$ | $WGM_2$ | $WP_4 \rightarrow WP_1 \rightarrow WP_3 \rightarrow WP_2$ | 18 |
| $RPO_2$ | $WGM_1$ | $WP_7$ | 7 |
| $RPO_3$ | $WGM_1$ | $WP_{11} \rightarrow WP_{12} \rightarrow WP_8 \rightarrow WP_5 \rightarrow WP_6 \rightarrow WP_9 \rightarrow WP_{10}$ | 23.2 |

a time-shift for each motion plan, in order to identify a coordinated motion plan avoiding collisions among robots, and granting the cell cycle time. Stage 3 is based on a mixed model mathematical problem.

A final simulation for the validation of the proposed cell design and motion plan is run in Stage 4.

Hereafter, inputs, outputs and the approach stages are described in details in terms of formalization and resolution algorithms.

## 4. Formalization and implementation

This section presents the formalization of the approach and a detailed description of the developed algorithms and methods. First, the required inputs and provided outputs are introduced; then, all the stages are analyzed.

### 4.1. Inputs and outputs of the methodology

Automotive company and OEM's inputs as well as generated outputs are hereafter described.

### 4.2. Stage 1 – single robot off-line motion planning

*Stage 1* of the approach (Fig. 2) aims at formalizing and solving the off-line motion planning for a single-robot assembly cell: for each couple $\left(RPO_{rpo}, WGM_{wgm}\right)$, the algorithm defines collision-free trajectories connecting the reachable welding points. The generated trajectories represent an input for Stages 2 and 3 of the proposed approach.

Because the environment is static and the problem can be considered a multi-goal problem,[2] probabilistic roadmaps (PRMs) with lazy collisions have been selected among the existing traditional approaches (Section 2.2). The calculus of the trajectory connecting the points of PRMs has been provided by integrating the motion planner of the robot actually used in the experimental phase (the ORL [35] – the motion planner from COMAU Robotics). Using such motion planner, the correspondence of simulated motion and the actual motion of real robots is extremely high. In comparison to state of the art (Section 2.2), PRM has been modified through the development of ad-hoc algorithms and criteria inspired to the technological problem of robotic spot welding. A detailed description of steps composing the Stage 1 is reported (Fig. 3).

**Table 8**
Industrial case – input – resource costs (for confidentiality issues the cost are fictional).

| Cost [€] | Value |
|---|---|
| $COST^{RM}$ | 20230 |
| $COST^{RSM}$ | 185000 |
| $COST^{WGM_{wgm}}$ | 8560 8790 9230 |

**Table 9**
Industrial case – input – possible combination of $\boldsymbol{RPO_{rpo}}$, $\boldsymbol{WGM_{wgm}}$.

| $RPO_{rpo}$ | $WGM_{wgm}$ | Initial joint pos [rad] |
|---|---|---|
| $RPO_1$ | $WGM_1$ | [0. 0 −0. 43 −1. 95 0. 0 0. 0 0. 0] |
| $RPO_2$ | $WGM_2$, $WGM_3$ | [0. 0 −0. 43 −1. 95 0. 0 0. 0 0. 0] |
| $RPO_3$ | $WGM_3$ | [0. 0 −0. 43 −1. 95 0. 0 0. 0 0. 0] |
| $RPO_4$ | $WGM_1$ | [0. 0 −0. 43 −1. 95 0. 0 0. 0 0. 0] |

#### 4.2.1. Stage 1i – definition of admissible welding points

Each welding point is identified by the Cartesian position ($x$, $y$, $z$), and by the axis orthogonal to the surface. Common accepted assumption is that the $z$-axis of the welding gun (i.e., the controlled closing axis) is orthogonal to the surface. Thus, the residual degrees of freedom for the welding gun pose are: the rotation around the $z$ axis, and the selection of the inverse kinematic solution among the feasible ones. Such degrees of freedom have been exploited to identify the 'best' robot pose for each welding point granting a collision-free robot configurations and the shortest path in the joint space between the initial and final configuration.

#### 4.2.2. Stage 1ii - Space sampling and obstacle-based sampling

The PRM points are sampled in the robot joint position space. The point sampling technique derives from Halton sequences [36], and it provides collision-free configuration check. The configuration workspace, where the points are generated, is the joint-space map corresponding to the cylinders in Cartesian space having as

**Table 7**
Industrial case – input – motion planning.

| $RPO_{rpo}$ | Initial joints [rad] | WP seq. |
|---|---|---|
| $RPO_1$ | [0. 0, – 0. 436, – 1. 95, 0. 0, 0. 0, 0. 0] | $WP_1 \rightarrow WP_2 \rightarrow WP_3 \rightarrow WP_4 \rightarrow WP_5 \rightarrow WP_6 \rightarrow WP_7$ |
| $RPO_2$ | [0. 0, – 0. 436, – 1. 95, 0. 0, 0. 0, 0. 0] | $WP_8 \rightarrow WP_9 \rightarrow WP_{10} \rightarrow WP_{11} \rightarrow WP_{12} \rightarrow WP_{13} \rightarrow WP_{14} \rightarrow WP_{15}$ |
| $RPO_3$ | [0. 0, – 0. 436, – 1. 95, 0. 0, 0. 0, 0. 0] | $WP_{16} \rightarrow WP_{17} \rightarrow WP_{18} \rightarrow WP_{19} \rightarrow WP_{20} \rightarrow WP_{21} \rightarrow WP_{22}$ |

[2] The number of queries is equal to the number of reachable welding point pairs

**Table 10**
Industrial case – solution.

| *RPO* | *WGM* | WP seq. | $OCT_{rpo}$ [s] |
|---|---|---|---|
| $RPO_4$ | $WGM_1$ | $WP_6 \rightarrow WP_2 \rightarrow WP_5 \rightarrow WP_7 \rightarrow WP_3 \rightarrow WP_4 \rightarrow WP_1$ | 28.32 |
| $RPO_2$ | $WGM_2$ | $WP_8 \rightarrow WP_9 \rightarrow WP_{13} \rightarrow WP_{11} \rightarrow WP_{15} \rightarrow WP_8 \rightarrow WP_{10} \rightarrow WP_{12} \rightarrow WP_{14}$ | 37.2 |
| $RPO_3$ | $WGM_3$ | $WP_{21} \rightarrow WP_{20} \rightarrow WP_{16} \rightarrow WP_{19} \rightarrow WP_{22} \rightarrow WP_{18} \rightarrow WP_{17}$ | 20.88 |

**Table 11**
Test case resolution time in hours.

| | Stage 1 | Stage 2 | Stage 3 | Stage 4 | Tot |
|---|---|---|---|---|---|
| Simplified case 1 | 10.51 | 1.25 | 86.79 | 1 | 99.55 |
| Simplified case 6 | 7.85 | 0.83 | 104.76 | 1 | 107.44 |
| Industrial case | 98 | 2.2 | 12 | 1 | 113.2 |

**Table 12**
Part A – Inputs (I) and outputs (O) of the approach of the stages (S).

| Symbol | Definition | S1 | S2 | S3 | S4 |
|---|---|---|---|---|---|
| *CBS* or *BIW* | See Table 1 | I | – | – | I |
| *BF* | See Table 1 | I | – | – | I |
| *BTD* | See Table 1 | I | – | – | I |
| *RM* | See Table 2 | I | I | I | I |
| *RSM* | See Table 2 | I | – | I | I |
| $RPO_{rpo}$, $rpo \in \{0, \ldots, N^{RPO}-1\}$ | See Table 2 | I | I | I | I |
| $WGM_{wgm}$, $wgm \in \{0, \ldots, N^{WGM}-1\}$ | See Table 2 | I | I | I | I |
| $WP_{wp}$, $wp \in \{0, \ldots, N^{WP}-1\}$ | See Table 1 | I | I | I | I |
| $RMP_{rmp}$, $rmp \in \{0, \ldots, N^{RMP}-1\}$ | See Table 4 | – | – | I | I |
| $NC^{RM} \in \mathbb{N}$ | See Table 2 | – | – | I | – |
| $NC^{WGM_{wgm}} \in \mathbb{N}$ | See Table 2 | – | – | I | – |
| $NC^{RSM} \in \{0, 1\}$ | See Table 2 | – | – | I | – |
| $COST^{RM} \in \mathbb{R}^+$ | See Table 2 | – | – | I | – |
| $COST^{WGM_{wgm}} \in \mathbb{R}^+$ | See Table 2 | – | – | I | – |
| $COST^{RSM} \in \mathbb{R}^+$ | See Table 2 | – | – | I | – |
| $MPf^{wgm,rpo}_{wp_1,wp_2} \in \{0, 1\}$ | See Table 4 | O | I | I | – |
| $MT^{wgm,rpo}_{wp_1,wp_2} \in \mathbb{R}^+$ | See Table 4 | O | I | I | – |
| $WT_{wp} \in \mathbb{R}^+$ | See Table 4 | – | – | I | – |
| $RCT \in \mathbb{R}^+$ | See Table 4 | – | – | I | – |
| $RWP \in \mathbb{N}$ | See Table 4 | – | – | I/O | – |
| $IGP_{rpo_1,rpo_2} \in \{0, 1\}$ | See Table 4 | – | – | I | – |
| $SP_{rpm_1,rpm_2} \in \{0, 1\}$ | See Table 4 | – | O | I | – |
| $UP_{rpm_1,rpm_2} \in \{0, 1\}$ | See Table 4 | – | O | I | – |
| *L* | See Table 4 | – | – | I | – |

**Table 13**
Part B – inputs (I) and outputs (O) of the approach of the stages (S).

| Symbol | Definition | S1 | S2 | S3 | S4 |
|---|---|---|---|---|---|
| $COST \in \mathbb{R}^+$ | See Table 3 | – | – | O | – |
| $TN^{RM} \in \mathbb{N}$ | See Table 3 | – | – | O | I |
| $TN^{WGM_{wgm}} \in \mathbb{N}$ | See Table 3 | – | – | O | I |
| $NA^{RM} \in \mathbb{N}$ | See Table 4 | – | – | O | – |
| $NA^{WGM_{wgm}} \in \mathbb{N}$ | See Table 4 | – | – | O | – |
| $NA^{RSM} \in \{0, 1\}$ | See Table 4 | – | – | O | – |
| $TN^{RM'} \in \mathbb{Z}$ | See Table 4 | – | – | O | – |
| $TN^{WGM'_{wgm}} \in \mathbb{Z}$ | See Table 4 | – | – | O | – |
| $RGP_{wgm,rpo} \in \{0, 1\}$ | See Table 3 | – | – | O | I |
| $MP^{wgm,rpo}_{wp_1,wp_2} \in \{0, 1\}$ | See Table 3 | – | – | O | I |
| $MPS^{wgm,rpo}_{wp_1,wp_2} \in \mathbb{N}$ | See Table 4 | – | – | O | I |
| $MTT^{wgm,rpo}_{wp_1,wp_2} \in \mathbb{R}^+$ | See Table 4 | – | – | O | I |
| $C^{wgm,rpo}_{wp_1,wp_2} \in \mathbb{R}^+$ | See Table 3 | – | – | O | I |
| $I^{wgm,rpo}_{wp_1,wp_2} \in \mathbb{R}^+$ | See Table 3 | – | – | O | I |
| $D^{wgm,rpo}_{wp_1,wp_2} \in \mathbb{R}^+$ | See Table 4 | – | – | O | I |
| $WPA_{rpo,wp} \in \{0, 1\}$ | See Table 3 | – | – | O | I |
| $OCT_{rpo} \in \mathbb{R}^+$ | See Table 3 | – | – | O | I |
| $MAXOCT \in \mathbb{R}^+$ | See Table 3 | – | – | O | I |
| $TP_{rpm_1,rpm_2} \in \{0, 1\}$ | See Table 4 | – | – | O | – |
| $SOP_{rpm_1,rpm_2} \in \{0, 1\}$ | See Table 4 | – | – | O | – |
| $ISP_{rpm_1,rpm_2} \in \{0, 1\}$ | See Table 4 | – | – | O | – |

**Table 14**
Simplified case – metal sheet position and orientation w.r.t. the cell reference frame.

| Rototraslation $R_{cell}$. Positions in [mm] |
|---|
| $[1, 0, 0, 0; 0, 1, 0, 0; 0, 0, 1, 650; 0, 0, 0, 1]$ |

axis the line connecting the robot initial position to reachable welding points or two welding points and as radius an appropriate value. Hereafter, the set of points in the joint space $\mathbf{q}_i$, $i = 1, \ldots, n$ composing the PRM is denoted as $\mathbf{v}$.

The generation of points through Halton sequences, however, guarantees good performance in the free space, while it displays some limitations in narrow passages. Thus, generation of points close to the *BIW* was achieved through the use of a developed obstacle-based technique sampling. The technique reduces the welding gun movements near the *BIW*, adding bound constraint for the orientation terns *a*, *e*, *r* and robot flags (i.e., the selection of the solution for the inverse kinematics of the robot among the feasible ones), Fig. 4.

*4.2.3. Stage 1iii – connection of the sampled points through motion planner*

Sampled points $\mathbf{v}$ are connected during Stage 1iii in order to obtain a roadmap. Connections $\mathbf{c}$ between the points $\mathbf{v}$ are provided by the ORL. The use of the ORL grants that the behavior of the robot in the simulated environment is coherent with the real behavior of the robot. Since PRM is based on lazy collision, the defined trajectories are not checked for collisions at this stage. Points are connected according to the *nearest-n* technique : each sampled point is connected to the nearest *n* points. The distance *D* between two points is evaluated accordingly to Euclidean norm $\|\cdot\|_2$ in the robot joint space.

The connectivity of the final roadmap, and the probability to successfully find a path, increases together with *n* as well as the computational time. [37] suggests to take $n = 15$ for probabilistic roadmap without lazy collision. However, the proposed approach is based on PRM with lazy collisions for which it is likely to employ a higher *n*. Indeed, this will reduce the possibility to have not-connected sub-roadmaps due to the deletion of all the connections during collision check.

*4.2.4. Stage 1iv – connection of the welding points to the roadmap*

During Stage 1iv, each reachable welding point is connected to the generated roadmap. First, the sampled point of the roadmap

**Table 15**
Simplified case – body fixture position and orientation w.r.t. the cell reference frame.

| Rototraslation $R_{cell}$. Positions in [mm] |
|---|
| [1, 0, 0, 1400; 0, 1, 0, 1200; 0, 0, 1, 0; 0, 0, 0, 1] |
| [1, 0, 0, – 1400; 0, 1, 0, 1200; 0, 0, 1, 0; 0, 0, 0, 1] |
| [1, 0, 0, 1400; 0, 1, 0, – 1200; 0, 0, 1, 0; 0, 0, 0, 1] |
| [1, 0, 0, 600; 0, 1, 0, 500; 0, 0, 1, 0; 0, 0, 0, 1] |
| [1, 0, 0, 600; 0, 1, 0, – 500; 0, 0, 1, 0; 0, 0, 0, 1] |
| [1, 0, 0, – 600; 0, 1, 0, 500; 0, 0, 1, 0; 0, 0, 0, 1] |
| [1, 0, 0, – 900; 0, 1, 0, 1200; 0, 0, 1, 0; 0, 0, 0, 1] |
| [1, 0, 0, – 1400; 0, 1, 0, 500; 0, 0, 1, 0; 0, 0, 0, 1] |
| [1, 0, 0, – 300; 0, 1, 0, 1200; 0, 0, 1, 0; 0, 0, 0, 1] |
| [1, 0, 0, – 1300; 0, 1, 0, – 1000; 0, 0, 1, 0; 0, 0, 0, 1] |
| [1, 0, 0, 800; 0, 1, 0, – 900; 0, 0, 1, 0; 0, 0, 0, 1] |
| [1, 0, 0, 500; 0, 1, 0, – 1100; 0, 0, 1, 0; 0, 0, 0, 1] |
| [1, 0, 0, 1300; 0, 1, 0, – 800; 0, 0, 1, 0; 0, 0, 0, 1] |
| [1, 0, 0, – 900; 0, 1, 0, 800; 0, 0, 1, 0; 0, 0, 0, 1] |
| [1, 0, 0, – 400; 0, 1, 0, – 800; 0, 0, 1, 0; 0, 0, 0, 1] |
| [1, 0, 0, 100; 0, 1, 0, – 800; 0, 0, 1, 0; 0, 0, 0, 1] |

nearest to the welding point is selected. If a collision-free path between the selected point and the welding point can be found by the motion planner, the points are connected. Otherwise, the second point nearest to the welding point will be selected and tested for collision-free path. The algorithm ends when a collision-free (both collisions with obstacles and robot self-collisions) connection is established. The collision is checked implementing a chord bisection strategy.

In order to reduce the probability to fail during the connections of the welding points to the roadmap, an ad-hoc motion planning constraint based on the industrial practice was introduced (Fig. 5). The algorithm tries to find out an escape linear path in the workspace gradually incrementing the distance from the welding point along the tool axis $-z$ (parallel to the axis normal to the surface in the welding point) and then along the tool axis $-x$.

#### *4.2.5. Stage 1v – search for collision-free path between selected welding points*

In Stage 1v, the collision-free path $\tau$ to move between two welding points $WP_i$, and $WP_j$ is defined. Specifically, the shortest path $\tau$ expressed as a sequence of points belonging to the roadmap is obtained through the use of the Dijkstra algorithm [38] (Fig. 6). Every path, thus every connection belonging to the path, has to be checked for possible collisions. If a path presents collisions, the connection responsible of the collision is deleted from the roadmap and a new path is searched.

Collision check, executed at sampled points along the predefined path, is based on OBB [39]. Specifically, at each time step the robot configuration is updated and checked for collisions. Since the robot models considered in this work present a hollow wrist, i.e. the robot cables run inside the robot, the behavior of the robot cables is not simulated.

**Table 16**
Simplified case – robot position and orientation.

| $RPO_{rpo}$ | $R^{cell}_{RPO_{rpo}}$ | Rot. about $Z_{RPO_{rpo}}$ [deg] | Initial joints [rad] |
|---|---|---|---|
| $RPO_1$ | [0, 1, 0, – 600; – 1, 0, 0, 4000; 0, 0, 1, 0; 0, 0, 0, 1] | 0 | [0, – 0. 436, – 1. 95, 0, 0, 0,] |
| $RPO_2$ | [1, 0, 0, – 2300; 0, 1, 0, 0; 0, 0, 1, 0; 0, 0, 0, 1] | 0 | [0, – 0. 436, – 1. 95, 0, 0, 0] |
| $RPO_3$ | [0, – 1, 0, 600; 1, 0, 0, – 4000; 0, 0, 1, 0; 0, 0, 0, 1] | 0 | [0, – 0. 436, – 1. 95, 0, 0, 0] |

**Table 17**
Simplified case – welding gun model – rototranslation expressed w.r.t. the cell reference frame.

| $WGM_{wgm}$ | $R^{WGM_{wgm}}_{WGM_{wgmCP}}$ | $R^{RPO_{rpoT}}_{WGM_{wgm}}$ |
|---|---|---|
| $WGM_1$ | $\begin{bmatrix} 1 & 0 & 0 & 1359.95 \\ 0 & 1 & 0 & 0 \\ 0 & 0 & 1 & 140.32 \\ 0 & 0 & 0 & 1 \end{bmatrix}$ | $\begin{bmatrix} 1 & 0 & 0 & 0 \\ 0 & 1 & 0 & 0 \\ 0 & 0 & 1 & 0 \\ 0 & 0 & 0 & 1 \end{bmatrix}$ |
| $WGM_2$ | $\begin{bmatrix} 0 & 1 & 0 & 0 \\ -1 & 0 & 0 & 1209.91 \\ 0 & 0 & 1 & 132.32 \\ 0 & 0 & 0 & 1 \end{bmatrix}$ | $\begin{bmatrix} 0 & -1 & 0 & 0 \\ 1 & 0 & 0 & 0 \\ 0 & 0 & 1 & 0 \\ 0 & 0 & 0 & 1 \end{bmatrix}$ |

**Table 18**
Simplified case – Center points of sampling areas for WPs w.r.t. the cell reference frame.

| Area | xyz [mm mm mm] |
|---|---|
| 1 | [–600 900 660] |
| 2 | [–700 –800 660] |
| 3 | [600 –800 660] |

**Table 19**
Simplified case 1 – welding points (expressed w.r.t. the cell reference frame, linear unit [mm], rotational unit [deg]).

| $WP_{wp}$ | x | y | z | a | e | r | Flag | Rotation about $Z_{WGM_{wgm}}$ [deg] | $WT_{wp}$ |
|---|---|---|---|---|---|---|---|---|---|
| $WP_1$ | –646.11 | –883.98 | 660.0 | 90 | 180 | 0 | – | 0 | 1.1 |
| $WP_2$ | –617.57 | 926.59 | 660.0 | 90 | 180 | –10 | – | 0 | 1.1 |
| $WP_3$ | –636.18 | 918.82 | 660.0 | 90 | 180 | –15 | – | 0 | 1.1 |
| $WP_4$ | –574.4 | 940.49 | 660.0 | 90 | 180 | –20 | – | 0 | 1.1 |
| $WP_5$ | –704.67 | –786.83 | 660.0 | 90 | 180 | 180 | – | 0 | 1.1 |
| $WP_6$ | –744.72 | –796.53 | 660.0 | 90 | 180 | 190 | – | 0 | 1.1 |
| $WP_7$ | –685.53 | –776.94 | 660.0 | 90 | 180 | 200 | – | 0 | 1.1 |
| $WP_8$ | –696.53 | –756.28 | 660.0 | 90 | 180 | 190 | – | 0 | 1.1 |
| $WP_9$ | –591.63 | –790.32 | 660.0 | 90 | 180 | 190 | – | 0 | 1.1 |
| $WP_{10}$ | 619.15 | –778.41 | 660.0 | 90 | 180 | 210 | – | 0 | 1.1 |
| $WP_{11}$ | 587.66 | –827.64 | 660.0 | 90 | 180 | 180 | – | 0 | 1.1 |
| $WP_{12}$ | 558.55 | –800.35 | 660.0 | 90 | 180 | 170 | – | 0 | 1.1 |

The recursive deletion of connections may lead to not-connected sub-roadmaps. These sub-roadmaps may occur when the welding point and the point to which it is connected are in a narrow passage. In such a case, the sampled point through which the welding point is connected to the roadmap is changed (*Stage 1iii*) till the sub-roadmap is escaped or all the sampled point have been tested. In such a case, the quality of the final path decreases but a solution may be available.

**Table 20**
Simplified case 2 – Welding points (expressed w.r.t. the cell reference frame, linear unit [mm], rotational unit [deg]).

| $WP_{wp}$ | x | y | z | a | e | r | Flag | Rotation about $Z_{WGM_{wgm}}$ [deg] | $WT_{wp}$ |
|---|---|---|---|---|---|---|---|---|---|
| $WP_1$ | −696.86 | 954.22 | 660.0 | 90 | 180 | 0 | – | 0 | 1.1 |
| $WP_2$ | −680.41 | 820.67 | 660.0 | 90 | 180 | -10 | – | 0 | 1.1 |
| $WP_3$ | −546.96 | 1008.67 | 660.0 | 90 | 180 | -15 | – | 0 | 1.1 |
| $WP_4$ | −507.83 | 812.20 | 660.0 | 90 | 180 | -20 | – | 0 | 1.1 |
| $WP_5$ | −608.10 | −868.33 | 660.0 | 90 | 180 | 180 | – | 0 | 1.1 |
| $WP_6$ | −615.59 | −702.61 | 660.0 | 90 | 180 | 190 | – | 0 | 1.1 |
| $WP_7$ | −579.91 | −740.68 | 660.0 | 90 | 180 | 200 | – | 0 | 1.1 |
| $WP_8$ | −792.57 | −809.30 | 660.0 | 90 | 180 | 190 | – | 0 | 1.1 |
| $WP_9$ | 656.47 | −730.47 | 660.0 | 90 | 180 | 190 | – | 0 | 1.1 |
| $WP_{10}$ | 507.19 | −917.73 | 660.0 | 90 | 180 | 210 | – | 0 | 1.1 |
| $WP_{11}$ | 660.98 | −725.91 | 660.0 | 90 | 180 | 180 | – | 0 | 1.1 |
| $WP_{12}$ | 587.59 | −781.51 | 660.0 | 90 | 180 | 170 | – | 0 | 1.1 |

#### 4.2.6. Stage 1vi – decreasing of the path length

Paths which are created by sampling-based method usually contain redundant motions. In *Stage 1vi*, the path pruning method [40] is applied to decrease path length. This technique assumes that a path $\tau$ is represented by a list of nodes $v_0,\ldots,v_{n-1}$ corresponding to the selected points $\mathbf{v}$ of the roadmap. Path pruning technique removes a node $v_{i+1}$ from the path $\tau$ if the path calculated by the motion planner (e.g., ORL) between nodes $v_i$ and $v_{i+2}$ is collision-free and shorter than the sum of the paths between $v_i$ and $v_{i+1}$ and between $v_{i+1}$ and $v_{i+2}$.

#### 4.2.7. Stage 1vii – generation of the collision-free trajectory

Stage 1vii allows the generation of the final collision-free trajectory connecting the selected welding points (Fig. 6(b)). Thus, the path $\tau$ found in *Stage 1vi* is passed to the motion planner (e.g., ORL). Each node of $\tau$ is a via-point with non-zero velocity and a blending parameter to manage the junction of two consecutive path segments. The process is iterative, since the blending of two consecutive segments introduces a deformation of the path checked in the previous step. Thus, an iterative procedure reduces the blending parameter till a final collision-free solution is found.

### 4.3. Stage 2 – off-line collision check of two-robot paths

Trajectories defined during Stage 1 are collision-free with respect to the obstacles in the environment, e.g. *BF*, *BIW*, *BTD*. However, these trajectories are generated disregarding the fact that they have to be executed in an environment shared with other robots. The aim of Stage 2 (Fig. 2) is to coordinate these trajectories. Thus, all the trajectories defined during Stage 1 are analyzed in couples. If no collisions can be found, the couple is declared safe; otherwise the couple is unsafe. In order to assess the safety of the couple, a volume-swept-like algorithm is employed [41]. Specifically, the idea is to test each configuration of the first robot along its path respect to each configuration of the second robot along its path (Fig. 7). With reference to the problem inputs and outputs presented in Appendix A, the information related to the safety of a couple is stored in the variables $SP_{rpm_1,rpm_2}$ and $UP_{rpm_1,rpm_2}$. If the couple is safe $SP_{rpm_1,rpm_2}$=1; otherwise $UP_{rpm_1,rpm_2}$=1.

As it was briefly explained in Section 3, the main limitation of such method consists on its independency from the time coordinate. Indeed, the definition of a couple of trajectories as unsafe does not necessarily mean that the robots executing those trajectories will collide. Indeed, some combinations of trajectory starting time may exist, that do not lead to any collisions. In other words, collisions of unsafe couple of trajectories could be avoided managing the synchronization of the robots through the modification of their starting time. Under the hypothesis of time independency, all these combinations, leading to a feasible motion planning, are discarded and not analyzed reducing the ability of the approach to find a feasible solution. However, the relaxation of the time-independency hypothesis during cell design and motion planning definition would have dramatically increased the model complexity and the resolution time of Stage 3. Some idea on how coping with this limitation is faced in future work section.

### 4.4. Stage 3 – multi-robot cell design and off-line motion planning

Stage 3 is based on linear mixed-integer mathematical model, formalized as a Traveling Salesman Problem.

In relation to the design problem, the model was developed accordingly to [42]. However, it represents a novelty in the approaches for the design of multi-robot assembly cell for spot welding since the application context and consecutively the majority of employed parameters, variables and constraints are inherently different.

Multi-robot coordination has been formulated as a decoupled motion planning approach, taking inspiration from jobshop scheduling problems. The linear mixed-integer mathematical model, therefore, is formulated as follows:

#### 4.4.1. Notation and parameters

The sets of elements that are necessary to model the problem together with their notation are reported in Table 4. Parameters and inputs are grouped into two areas: process and resource areas. The remaining data consist of generic parameters.

#### 4.4.2. Decision variables

The set of decision variables can be divided into three groups as shown in Table 4.

#### 4.4.3. Objective function and constraints

The objective function (Eq. (1)) of the model aims at minimizing the expected costs of the cell. This cost is related to the acquired resources: robots, welding guns and robot support structure. Cell whole-life costs or life-cycle costs (e.g. energy consumption, maintenance, etc.) are not considered in this work.

$$minimize\ \ COST \tag{1}$$

#### 4.4.4. Resource constraints

Constraints Eqs. (2)–(11) define the number of robots, welding guns and robot support structures to be acquired as well as the position/orientation of the robots and the allocation of the welding

**Table 21**
Simplified case 2 – solution.

| *RPO* | *WGM* | WP seq. | $OCT_{rpo}$ [s] |
|---|---|---|---|
| $RPO_1$ | $WGM_2$ | $WP_3 \rightarrow WP_4 \rightarrow WP_2 \rightarrow WP_1$ | 19.07 |
| $RPO_3$ | $WGM_1$ | $WP_{12} \rightarrow WP_{11} \rightarrow WP_5 \rightarrow WP_9 \rightarrow WP_8 \rightarrow WP_6 \rightarrow WP_7 \rightarrow WP_{10}$ | 24.72 |

**Table 22**
Simplified case 3 – welding points (expressed w.r.t. the cell reference frame, linear unit [mm], rotational unit [deg]).

| $WP_{wp}$ | x | y | z | a | e | r | Flag | Rotation about $Z_{WGM_{wgm}}$ [deg] | $WT_{wp}$ |
|---|---|---|---|---|---|---|---|---|---|
| $WP_1$ | −431.12 | 791.23 | 660.0 | 90 | 180 | 0 | – | 0 | 1.1 |
| $WP_2$ | −483.96 | 994.17 | 660.0 | 90 | 180 | −10 | – | 0 | 1.1 |
| $WP_3$ | −503.34 | 916.19 | 660.0 | 90 | 180 | −15 | – | 0 | 1.1 |
| $WP_4$ | −371.69 | 933.89 | 660.0 | 90 | 180 | −20 | – | 0 | 1.1 |
| $WP_5$ | −747.24 | −965.15 | 660.0 | 90 | 180 | 180 | – | 0 | 1.1 |
| $WP_6$ | −503.14 | −914.05 | 660.0 | 90 | 180 | 190 | – | 0 | 1.1 |
| $WP_7$ | −611.89 | −776.63 | 660.0 | 90 | 180 | 200 | – | 0 | 1.1 |
| $WP_8$ | −698.42 | −854.20 | 660.0 | 90 | 180 | 190 | – | 0 | 1.1 |
| $WP_9$ | 356.77 | −793.13 | 660.0 | 90 | 180 | 190 | – | 0 | 1.1 |
| $WP_{10}$ | 634.45 | −949.72 | 660.0 | 90 | 180 | 210 | – | 0 | 1.1 |
| $WP_{11}$ | 387.543689 | −740.92 | 660.0 | 90 | 180 | 180 | – | 0 | 1.1 |
| $WP_{12}$ | 610.503143 | −843.27 | 660.0 | 90 | 180 | 170 | – | 0 | 1.1 |

**Table 23**
Simplified case 3 – solution.

| $RPO$ | $WGM$ | WP seq. | $OCT_{rpo}$ [s] |
|---|---|---|---|
| $RPO_1$ | $WGM_2$ | $WP_2 \rightarrow WP_4 \rightarrow WP_1 \rightarrow WP_3$ | 20.19 |
| $RPO_2$ | $WGM_1$ | $WP_7 \rightarrow WP_8$ | 10.32 |
| $RPO_3$ | $WGM_1$ | $WP_{12} \rightarrow WP_{11} \rightarrow WP_{10} \rightarrow WP_5 \rightarrow WP_6 \rightarrow WP_9$ | 20.24 |

**Table 24**
Simplified case 4 – welding points (expressed w.r.t. the cell reference frame, linear unit [mm], rotational unit [deg]).

| $WP_{wp}$ | x | y | z | a | e | r | Flag | Rotation about $Z_{WGM_{wgm}}$ [deg] | $WT_{wp}$ |
|---|---|---|---|---|---|---|---|---|---|
| $WP_1$ | −519.75 | 1185.70 | 660.0 | 90 | 180 | 0 | – | 0 | 1.1 |
| $WP_2$ | −547.46 | 1170.36 | 660.0 | 90 | 180 | −10 | – | 0 | 1.1 |
| $WP_3$ | −579.58 | 977.88 | 660.0 | 90 | 180 | −15 | – | 0 | 1.1 |
| $WP_4$ | −430.19 | 967.19 | 660.0 | 90 | 180 | −20 | – | 0 | 1.1 |
| $WP_5$ | −715.48 | −1127.84 | 660.0 | 90 | 180 | 180 | – | 0 | 1.1 |
| $WP_6$ | −1019.98 | −840.12 | 660.0 | 90 | 180 | 190 | – | 0 | 1.1 |
| $WP_7$ | −585.07 | −1112.06 | 660.0 | 90 | 180 | 200 | – | 0 | 1.1 |
| $WP_8$ | −776.57 | −591.65 | 660.0 | 90 | 180 | 190 | – | 0 | 1.1 |
| $WP_9$ | 488.83 | −595.27 | 660.0 | 90 | 180 | 190 | – | 0 | 1.1 |
| $WP_{10}$ | 575.22 | −1060.56 | 660.0 | 90 | 180 | 210 | – | 0 | 1.1 |
| $WP_{11}$ | 503.96 | −674.21 | 660.0 | 90 | 180 | 180 | – | 0 | 1.1 |
| $WP_{12}$ | 813.74 | −1021.64 | 660.0 | 90 | 180 | 170 | – | 0 | 1.1 |

**Table 25**
Simplified case 4 – solution.

| $RPO$ | $WGM$ | WP seq. | $OCT_{rpo}$ [s] |
|---|---|---|---|
| $RPO_1$ | $WGM_2$ | $WP_1 \rightarrow WP_2 \rightarrow WP_4$ | 10.42 |
| $RPO_2$ | $WGM_1$ | $WP_7 \rightarrow WP_8 \rightarrow WP_6 \rightarrow WP_3$ | 17.64 |
| $RPO_3$ | $WGM_1$ | $WP_9 \rightarrow WP_{10} \rightarrow WP_{11} \rightarrow WP_{12} \rightarrow WP_5$ | 20.15 |

guns to the robots. Specifically, constraint Eqs. ((2)–7) define the relation among the number and model of robots, guns and structure acquired and to be acquired.[3] Constraint Eq. (8) imposes that the total number of selected welding guns is equal to the total number of robots. Similarly, constraint Eq. (9) describes an equality between the number of robots and the number of

[3] Acquired resources are the difference between the number of resources estimated by the final cell design minus the number of resources owned by the company

**Table 26**
Simplified case 5 – welding points (expressed w.r.t. the cell reference frame, linear unit [mm], rotational unit [deg]).

| $WP_{wp}$ | x | y | z | a | e | r | Flag | Rotation about $Z_{WGM_{wgm}}$ [deg] | $WT_{wp}$ |
|---|---|---|---|---|---|---|---|---|---|
| $WP_1$ | −519.75 | 1085.70 | 660.0 | 90 | 180 | 0 | – | 0 | 1.1 |
| $WP_2$ | −616.06 | 1042.48 | 660.0 | 90 | 180 | −10 | – | 0 | 1.1 |
| $WP_3$ | −579.58 | 977.88 | 660.0 | 90 | 180 | −15 | – | 0 | 1.1 |
| $WP_4$ | −430.19 | 967.19 | 660.0 | 90 | 180 | −20 | – | 0 | 1.1 |
| $WP_5$ | −715.48 | −1127.84 | 660.0 | 90 | 180 | 180 | – | 0 | 1.1 |
| $WP_6$ | −1019.98 | −840.12 | 660.0 | 90 | 180 | 190 | – | 0 | 1.1 |
| $WP_7$ | −585.07 | −1112.06 | 660.0 | 90 | 180 | 200 | – | 0 | 1.1 |
| $WP_8$ | −776.57 | −591.65 | 660.0 | 90 | 180 | 190 | – | 0 | 1.1 |
| $WP_9$ | 488.83 | −595.27 | 660.0 | 90 | 180 | 190 | – | 0 | 1.1 |
| $WP_{10}$ | 560.23 | −959.56 | 660.0 | 90 | 180 | 210 | – | 0 | 1.1 |
| $WP_{11}$ | 501.56 | −653.11 | 660.0 | 90 | 180 | 180 | – | 0 | 1.1 |
| $WP_{12}$ | 823.54 | −1025.55 | 660.0 | 90 | 180 | 170 | – | 0 | 1.1 |

**Table 27**
Simplified case 5 – solution.

| $RPO$ | $WGM$ | WP seq. | $OCT_{rpo}$ [s] |
|---|---|---|---|
| $RPO_1$ | $WGM_2$ | $WP_1 \rightarrow WP_4$ | 9.61 |
| $RPO_2$ | $WGM_1$ | $WP_8 \rightarrow WP_7 \rightarrow WP_6 \rightarrow WP_3 \rightarrow WP_2$ | 19.90 |
| $RPO_3$ | $WGM_1$ | $WP_{11} \rightarrow WP_9 \rightarrow WP_{10} \rightarrow WP_5 \rightarrow WP_{12}$ | 19.90 |

**Table 28**
Simplified case 6 – welding points (expressed w.r.t. the cell reference frame, linear unit [mm], rotational unit [deg]).

| $WP_{wp}$ | x | y | z | a | e | r | Flag | Rotation about $Z_{WGM_{wgm}}$ [deg] | $WT_{wp}$ |
|---|---|---|---|---|---|---|---|---|---|
| $WP_1$ | −568.44 | 85.90 | 660.0 | 90 | 180 | 0 | – | 0 | 1.1 |
| $WP_2$ | −543.33 | 1007.93 | 660.0 | 90 | 180 | −10 | – | 0 | 1.1 |
| $WP_3$ | −584.80 | 1103.83 | 660.0 | 90 | 180 | −15 | – | 0 | 1.1 |
| $WP_4$ | −471.66 | 954.68 | 660.0 | 90 | 180 | −20 | – | 0 | 1.1 |
| $WP_5$ | −1112.69 | −851.34 | 660.0 | 90 | 180 | 180 | – | 0 | 1.1 |
| $WP_6$ | −889.40 | −1096.95 | 660.0 | 90 | 180 | 190 | – | 0 | 1.1 |
| $WP_7$ | −577.73 | −1050.69 | 660.0 | 90 | 180 | 200 | – | 0 | 1.1 |
| $WP_8$ | −696.53 | −756.28 | 660.0 | 90 | 180 | 190 | – | 0 | 1.1 |
| $WP_9$ | −696.53 | −756.28 | 660.0 | 90 | 180 | 190 | – | 0 | 1.1 |
| $WP_{10}$ | 1028.97 | −918.12 | 660.0 | 90 | 180 | 210 | – | 0 | 1.1 |
| $WP_{11}$ | 1028.97 | −918.12 | 660.0 | 90 | 180 | 180 | – | 0 | 1.1 |
| $WP_{12}$ | 288.78 | −854.74 | 660.0 | 90 | 180 | 170 | – | 0 | 1.1 |

**Table 29**
Simplified case 6 – solution.

| *RPO* | *WGM* | WP seq. | $OCT_{rpo}$ [s] |
|---|---|---|---|
| $RPO_1$ | $WGM_2$ | $WP_3 \rightarrow WP_4 \rightarrow WP_1 \rightarrow WP_2$ | 17.05 |
| $RPO_2$ | $WGM_1$ | $WP_8 \rightarrow WP_7 \rightarrow WP_5 \rightarrow WP_6$ | 14 |
| $RPO_3$ | $WGM_1$ | $WP_9 \rightarrow WP_{12} \rightarrow WP_{11} \rightarrow WP_{10}$ | 17.05 |

**Table 30**
Simplified case 7 – welding points (expressed w.r.t. the cell reference frame, linear unit [mm], rotational unit [deg]).

| $WP_{wp}$ | x | y | z | a | e | r | Flag | Rotation about $Z_{WGM_{wgm}}$ [deg] | $WT_{wp}$ |
|---|---|---|---|---|---|---|---|---|---|
| $WP_1$ | −519.87 | 1014.91 | 660.0 | 90 | 180 | 0 | – | 0 | 1.1 |
| $WP_2$ | 12.65 | 926.55 | 660.0 | 90 | 180 | −10 | – | 0 | 1.1 |
| $WP_3$ | −1081.58 | 640.43 | 660.0 | 90 | 180 | −15 | – | 0 | 1.1 |
| $WP_4$ | −473.72 | 1029.51 | 660.0 | 90 | 180 | −20 | – | 0 | 1.1 |
| $WP_5$ | −1093.10 | −721.58 | 660.0 | 90 | 180 | 180 | – | 0 | 1.1 |
| $WP_6$ | −825.57 | −513.83 | 660.0 | 90 | 180 | 190 | – | 0 | 1.1 |
| $WP_7$ | −797.01 | −704.68 | 660.0 | 90 | 180 | 200 | – | 0 | 1.1 |
| $WP_8$ | −727.56 | −700.24 | 660.0 | 90 | 180 | 190 | – | 0 | 1.1 |
| $WP_9$ | 1169.20 | −540.61 | 660.0 | 90 | 180 | 190 | – | 0 | 1.1 |
| $WP_{10}$ | 981.23 | −1082.18 | 660.0 | 90 | 180 | 210 | – | 0 | 1.1 |
| $WP_{11}$ | 1047.20 | −1062.46 | 660.0 | 90 | 180 | 180 | – | 0 | 1.1 |
| $WP_{12}$ | 11.44 | −1034.77 | 660.0 | 90 | 180 | 170 | – | 0 | 1.1 |

**Table 31**
Simplified case 7 – solution.

| *RPO* | *WGM* | WP seq. | $OCT_{rpo}$ [s] |
|---|---|---|---|
| $RPO_1$ | $WGM_2$ | $WP_1 \rightarrow WP_2 \rightarrow WP_4 \rightarrow WP_3$ | 20.90 |
| $RPO_2$ | $WGM_1$ | $WP_7 \rightarrow WP_6$ | 13.80 |
| $RPO_3$ | $WGM_1$ | $WP_{12} \rightarrow WP_{11} \rightarrow WP_9 \rightarrow WP_{19} \rightarrow WP_5 \rightarrow WP_8$ | 21.28 |

selected robots. Since different gun models can be selected, Eq. (10) constraints the number of selected welding guns for each type. Eq. (11) prevents the selection of two robots in the same position.

$$COST = NA^{RM} \cdot COST^{RM} + \sum_{wgm} \left( NA^{WGM_{wgm}} \cdot COST^{WGM_{wgm}} \right) + NA^{RSM} \cdot COST^{RSM} \quad (2)$$

$$TN^{RM'} = TN^{RM} - NC^{RM} \quad (3)$$

$$NA^{RM} \geq TN^{RM'} \quad (4)$$

$$TN^{WGM'_{wgm}} = TN^{WGM_{wgm}} - NC^{WGM_{wgm}} \quad \forall\, wgm \quad (5)$$

$$NA^{WGM_{wgm}} \geq TN^{WGM'_{wgm}} \quad \forall wgm \quad (6)$$

$$NA^{RSM} = 1 - NC^{RSM} \quad (7)$$

$$TN^{RM} = \sum_{wgm} TN^{WGM_{wgm}} \quad (8)$$

$$TN^{RM} \geq \sum_{wgm,rpo} RGP_{wgm,rpo} \quad (9)$$

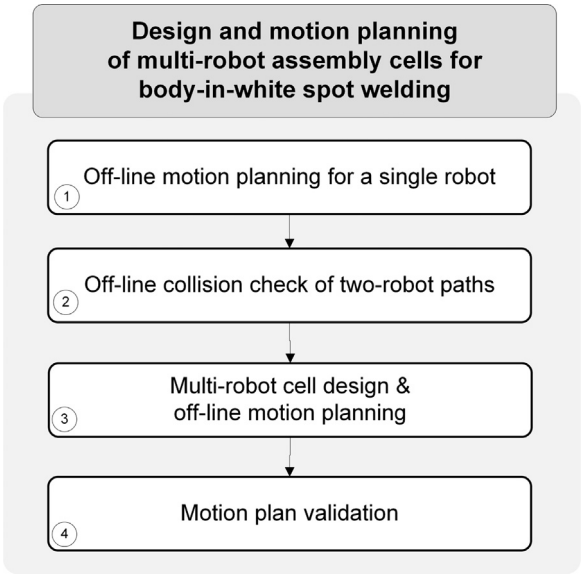


**Fig. 2.** The proposed method.

$$TN^{WGM_{wgm}} = \sum_{rpo} RGP_{wgm,rpo} \quad \forall wgm \quad (10)$$

$$1 \geq \left( \sum_{wgm} RGP_{wgm,rpo_1} \right) + \left( \sum_{wgm} RGP_{wgm,rpo_2} \right) \cdot IGP_{rpo_1,rpo_2} \quad \forall rpo_1, rpo_2 \quad (11)$$

#### 4.4.5. Motion planning constraints

Constraints Eqs. (12)–(23) grant the coherence among the variable related to the robot motion plan. Specifically, Eqs. (12) and (13) state that for each robot position/orientation to which a welding point is associated, a welding gun has to be selected. Constraint Eq. (14) imposes the allocation of each welding point to one robot position/orientation with exception of the welding point $wp = 0$ (the robot initial position). Indeed, every robot has its own starting position (15). Moreover, the fictitious welding point, i.e. the point representing the initial position of the robot end effector, is the first to be executed (Eq. 21). Constraints Eqs. (16), (17), (19), and (20) define the allocation of the welding points/welding guns to the robot positions/orientations and the motion plan related to each robot/welding guns. Indeed, if a position/orientation is not activated (no robot and welding guns are associated), no motion plan has to be defined and no welding gun has to be associated. Besides, these constraints are related to the formal definition of the motion plan for each position/orientation: for each position/orientation, every welding point can be executed only once. Constraint Eq. (18) defines the motion plan taking into account the information related to existing collision-free trajectory between two welding points. Constraint Eq. (22) allows the temporization of the motion plan for each position/orientation: thus, for each robot, the sequence of execution of the welding points is given. Variables related to the welding point sequence ($MPS$) have to be coherent with variables related to the trajectory selection and trajectory feasibility ($MP$) (constraint Eq. (23)). Constraints Eqs. (24)–(30) evaluate the initial and final time for the execution of the selected trajectories. Constraint Eq. (24) defines the initial time of each selected trajectory. Constraint Eq. (25) grants the temporal coherence among the completion and starting time of subsequent trajectories. Constraint Eqs. (26)–(28) lead to the coherence among the variable related to trajectory completion, starting, delay time and the motion plan: if a trajectory is not selected, its completion time, starting time and delay have to be null. Constraint Eqs. (29)

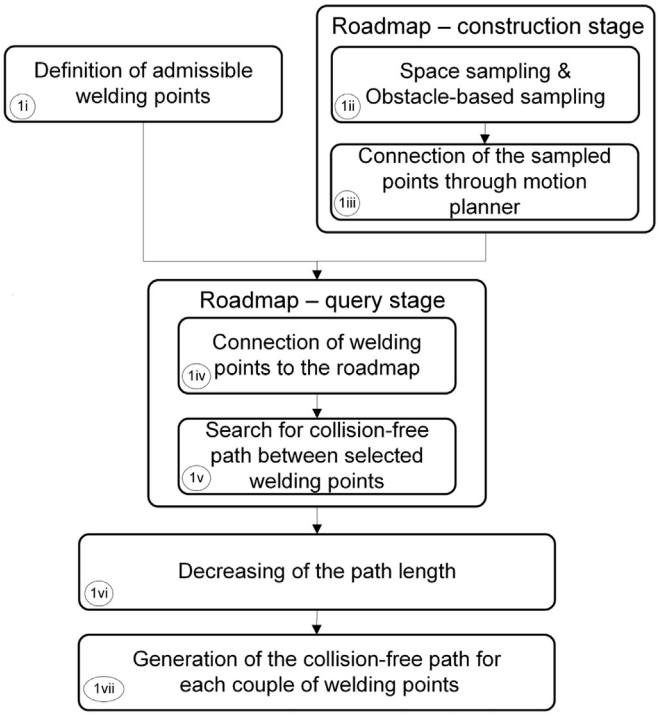


**Fig. 3.** Approach schema (Stage 1).

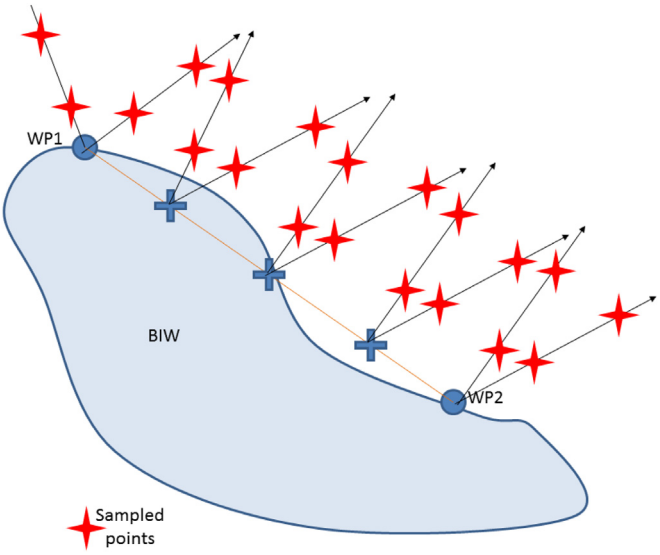


**Fig. 4.** *WPs*-based sampling: the light-blue element represents the metal sheets/body-in-white (Stage 1ii).

and (30) present the equations for the evaluation of the completion time and execution time. Finally, thanks to Eqs. (31)–(37), the motion plan coordination is granted.

$$\sum_{wp} WPA_{rpo,wp} \cdot L \leq \sum_{wgm} RGP_{wgm,rpo} \;\forall\; rpo \tag{12}$$

$$\sum_{wp} WPA_{rpo,wp} \geq \sum_{wgm} RGP_{wgm,rpo} \;\forall\; rpo \tag{13}$$

$$\sum_{rpo} WPA_{rpo,wp}=1 \qquad wp\neq 0 \vee wp < N^{WP} - RWP \tag{14}$$

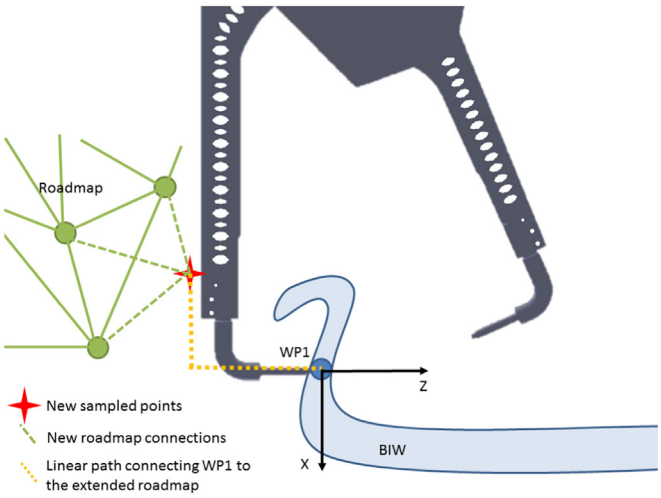


**Fig. 5.** Auxiliary strategy to connect welding points to the PRM (Stage 1iv).

$$\sum_{rpo} WPA_{rpo,0} = TN^{RM} \tag{15}$$

$$\sum_{wgm,wp_2} MP^{wgm,rpo}_{wp,wp_2} = WPA_{rpo,wp} \quad \forall rpo,\, wp \tag{16}$$

$$\sum_{wgm,wp_1} MP^{wgm,rpo}_{wp_1,wp} = WPA_{rpo,wp} \quad \forall rpo,\, wp \tag{17}$$

$$MP^{wgm,rpo}_{wp_1,wp_2} \leq MPf^{wgm,rpo}_{wp_1,wp_2} \quad \forall wgm,\, rpo,\, wp_1,\, wp_2 \tag{18}$$

$$\sum_{wp_1,wp_2} MP^{wgm,rpo}_{wp_1,wp_2} \cdot L \leq RGP_{wgm,rpo} \quad \forall wgm,\, rpo \tag{19}$$

$$\sum_{wp_1,wp_2} MP^{wgm,rpo}_{wp_1,wp_2} \geq RGP_{wgm,rpo} \quad \forall wgm,\, rpo \tag{20}$$

$$\sum_{wp} MPS^{wgm,rpo}_{0,wp} = RGP_{wgm,rpo} \quad \forall wgm,\, rpo \tag{21}$$

$$WPA_{rpo,wp} = \sum_{wgm,wp_2} MPS^{wgm,rpo}_{wp,wp_2} - \sum_{wgm,wp_1} MPS^{wgm,rpo}_{wp_1,wp} \;\forall\; rpo,\, wp\neq 0 \tag{22}$$

$$MP^{wgm,rpo}_{wp_1,wp_2} \geq \frac{MPS^{wgm,rpo}_{wp_1,wp_2}}{N^{WP}} \;\forall\; wgm,\, rpo,\, wp_1,\, wp_2 \tag{23}$$

$$I^{wgm,rpo}_{0,wp_2}=0 \quad \forall wgm,\, rpo,\, wp_2 \tag{24}$$

$$\sum_{wp_3} I^{wgm,rpo}_{wp_2,wp_3} = \sum_{wp_1} C^{wgm,rpo}_{wp_1,wp_2}, \quad \forall wgm,\, rpo,\, wp_2\neq 0 \tag{25}$$

$$L \cdot I^{wgm,rpo}_{wp_1,wp_2} \leq MP^{wgm,rpo}_{wp_1,wp_2} \quad \forall wgm,\, rpo,\, wp_1,\, wp_2 \tag{26}$$

$$L \cdot C^{wgm,rpo}_{wp_1,wp_2} \leq MP^{wgm,rpo}_{wp_1,wp_2} \quad \forall wgm,\, rpo,\, wp_1,\, wp_2 \tag{27}$$

$$L \cdot D^{wgm,rpo}_{wp_1,wp_2} \leq MP^{wgm,rpo}_{wp_1,wp_2} \quad \forall wgm,\, rpo,\, wp_1,\, wp_2 \tag{28}$$

$$C^{wgm,rpo}_{wp_1,wp_2} = I^{wgm,rpo}_{wp_1,wp_2} + MTT^{wgm,rpo}_{wp_1,wp_2} + D^{wgm,rpo}_{wp_1,wp_2} \;\forall\; wgm,\, rpo,\, wp_1,\, wp_2 \tag{29}$$

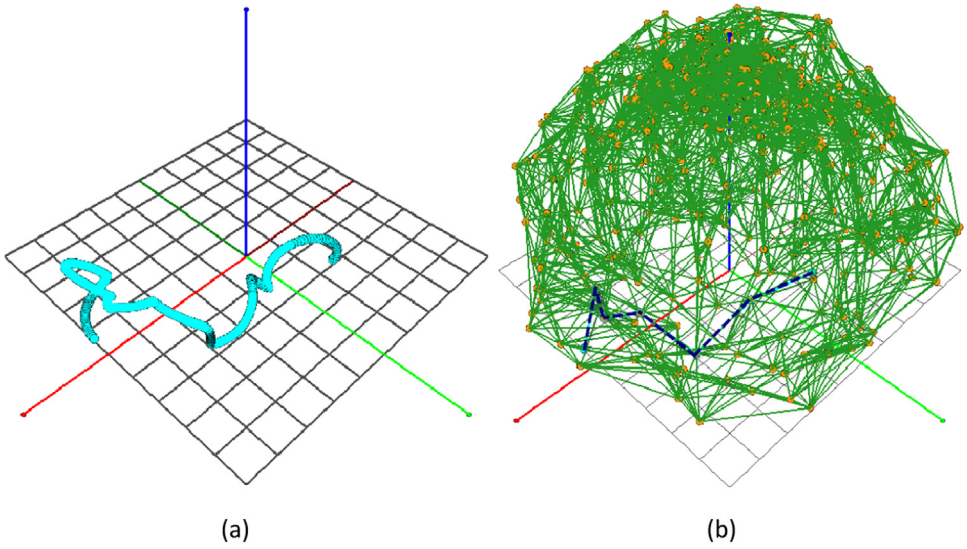


**Fig. 6.** Query roadmap for single-robot (Stage 1v).

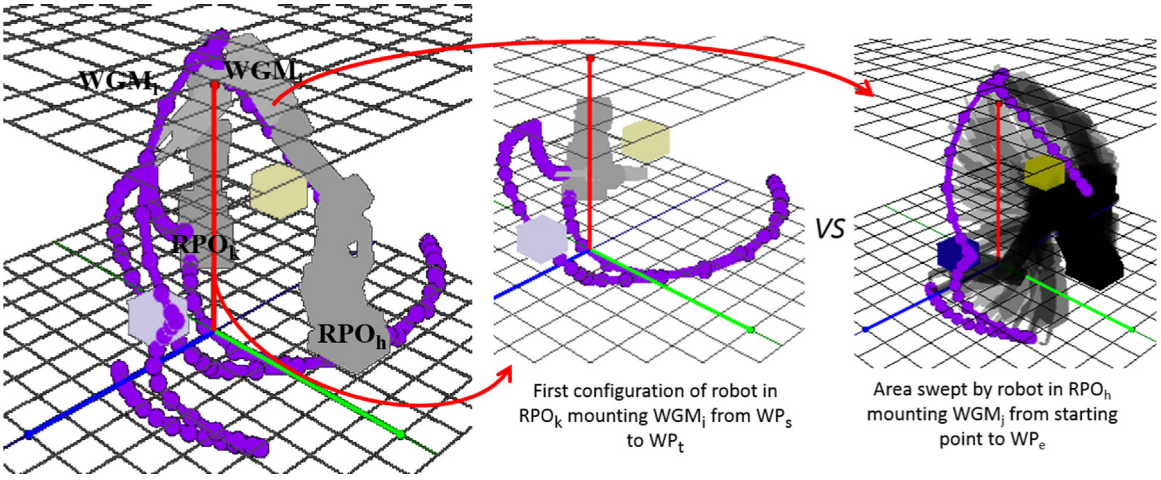


**Fig. 7.** Stage 2 – volume swept-like algorithm.

$$MTT^{wgm,rpo}_{wp_1,wp_2} = MP^{wgm,rpo}_{wp_1,wp_2} \cdot MT^{wgm,rpo}_{wp_1,wp_2} + WT_{wp_2} \cdot MP^{wgm,rpo}_{wp_1,wp_2} \quad \forall wgm, rpo, wp_1, wp_2 \tag{30}$$

$$\begin{cases} A = MPf_{wgm^{rpm_1},rpo^{rpm_1},wp_1^{rpm_1},wp_2^{rpm_1}} \cdot MPf_{wgm^{rpm_2},rpo^{rpm_2},wp_1^{rpm_2},wp_2^{rpm_2}}\left(SP_{rpm_1,rpm_2} + UP_{rpm_1,rpm_2}\right)TP_{rpm_1,rpm_2} \\ B = \left(\frac{C_{wgm^{rpm_1},rpo^{rpm_1},wp_1^{rpm_1},wp_2^{rpm_1}}}{2\,RCT}\right) - \left(\frac{I_{wgm^{rpm_2},rpo^{rpm_2},wp_1^{rpm_2},wp_2^{rpm_2}}}{2\,RCT} + L\right) \cdot MPf_{wgm^{rpm_1},rpo^{rpm_1},wp_1^{rpm_1},wp_2^{rpm_1}} \cdot MPf_{wgm^{rpm_2},rpo^{rpm_2},wp_1^{rpm_2},wp_2^{rpm_2}} \cdot \left(SP_{rpm_1,rpm_2} + UP_{rpm_1,rpm_2}\right) \\ A \geq B \quad \forall rmp_1, rmp_2 \end{cases} \tag{31}$$

$$\begin{cases} A = MPf_{wgm^{rpm_1},rpo^{rpm_1},wp_1^{rpm_1},wp_2^{rpm_1}} \cdot MPf_{wgm^{rpm_2},rpo^{rpm_2},wp_1^{rpm_2},wp_2^{rpm_2}}\left(SP_{rpm_1,rpm_2} + UP_{rpm_1,rpm_2}\right)TP_{rpm_1,rpm_2} \\ B = \left(\frac{C_{wgm^{rpm_1},rpo^{rpm_1},wp_1^{rpm_1},wp_2^{rpm_1}}}{2\,RCT}\right) - \left(\frac{I_{wgm^{rpm_2},rpo^{rpm_2},wp_1^{rpm_2},wp_2^{rpm_2}}}{2\,RCT} - 1\right) \cdot MPf_{wgm^{rpm_1},rpo^{rpm_1},wp_1^{rpm_1},wp_2^{rpm_1}} \cdot MPf_{wgm^{rpm_2},rpo^{rpm_2},wp_1^{rpm_2},wp_2^{rpm_2}} \cdot \left(SP_{rpm_1,rpm_2} + UP_{rpm_1,rpm_2}\right) \\ A \leq B \quad \forall rmp_1, rmp_2 \end{cases} \tag{32}$$

$$TP_{rpm_1,rpm_2} \leq (SP_{rpm_1,rpm_2} + UP_{rpm_1,rpm_2})MPf_{wgm^{rpm_1},rpo^{rpm_1},wp_1^{rpm_1},wp_2^{rpm_1}} \cdot MPf_{wgm^{rpm_2},rpo^{rpm_2},wp_1^{rpm_2},wp_2^{rpm_2}} \quad \forall rmp_1, rmp_2 \tag{33}$$

$$SOP_{rpm_1,rpm_2} \leq \frac{TP_{rpm_1,rpm_2} + TP_{rpm_2,rpm_1}}{4} + \frac{MP_{wgm^{rpm_1},rpo^{rpm_1},wp_1^{rpm_1},wp_2^{rpm_1}}}{4} + \frac{MP_{wgm^{rpm_2},rpo^{rpm_2},wp_1^{rpm_2},wp_2^{rpm_2}}}{4} \quad \forall\, rmp_1, rmp_2 \mid rmp_1 \neq rmp_2 \tag{34}$$

$$SOP_{rpm_1,rpm_2} \geq TP_{rpm_1,rpm_2} + TP_{rpm_2,rpm_1} + MP_{wgm^{rpm_1},rpo^{rpm_1},wp_1^{rpm_1},wp_2^{rpm_1}} + MP_{wgm^{rpm_2},rpo^{rpm_2},wp_1^{rpm_2},wp_2^{rpm_2}} - 4 + L \quad \forall rmp_1, rmp_2 \mid rmp_1 \neq rmp_2 \tag{35}$$

$$ISP_{rpm_1,rpm_2} \leq SP_{rpm_1,rpm_2} \;\forall\; rmp_1, rmp_2 \tag{36}$$

$$ISP_{rpm_1,rpm_2} \geq SOP_{rpm_1,rpm_2} \;\forall\; rmp_1, rmp_2 \tag{37}$$

#### 4.4.6. Cycle time constraints

Constraints Eqs. (38)–(40) evaluate the cell cycle time. Specifically, constraint Eq. (38) evaluates the cycle time for each robot, while constraint Eq. (39) defines the cycle time of the assembly cell. Besides, constraint Eq. (40) imposes that the obtained cycle time is lower that the required cycle time.

$$OCT_{rpo} \geq C_{wp_1,wp_2}^{wgm,rpo} \quad \forall wgm, rpo, wp_1, wp_2 \tag{38}$$

$$OCT_{rpo} \leq MAXOCT \quad \forall rpo \tag{39}$$

$$MAXOCT \leq RCT \tag{40}$$

#### 4.4.7. Resolution

The model could report an infeasibility problem when:

1. at least one welding point is not reachable;
2. all the points are reachable but this will require the selection of robots in the same position and a different orientation;
3. it is not possible to identifying at least one welding sequence requiring the visit of the welding points and the robot initial position only once;
4. it is not possible to coordinate the robot in the given cycle time.

Points 1–3 require the modification of the input data (robot positions/orientations). However, such infeasible condition is unlikely to occur, since it is based on the experience of the worker. On the contrary, the last cause of infeasibility presents higher probability to occur since it depends from the inputs of the automobile company. In such a case, it is important to identify the cycle time according to which the mathematical model is able to provide a solution. Thus, when an infeasibility problem is achieved, an additional iterative algorithm is provided as a further solving step (Fig. 8). Specifically, a solution is sought removing any temporal constraint (i.e., with an infinitive cycle time). If this results to the elimination of the infeasibility problem, the problem will be iteratively solved increasing the required cycle time at each step, till a feasible solution is identified. If the infeasibility problem remains, since in the Traveling Salesman Problem each node can be passed only once, the number of robot-starting-configuration replica is increased in order to allow the robot to have at disposal a resting position without collision with the other. Once the necessary number of replica is identified, the iterative process for the identification of required cycle time starts.

### 4.5. Stage 4 – motion plan validation

Motion plan validation (Stage 4 in Fig. 2) consists in the simulation of the results produced by Stage 3. The generated cell design is set and the robots execute the defined motion plan. During the simulation, the absence of active and passive collision is checked.

### 4.6. Implementation

The proposed approach was implemented in a C++ software tool structured in 12 libraries. Where possible, commercial or open-source libraries were used: RAPID [39] - decomposition of the environment in oriented bounding boxes (OBBs) and collision detection, OpenGL [43] - graphical interface, ORL [35] - trajectory planner for COMAU robots, Cplex [44] - resolution of the mathematical model presented in Section 4.4 and BzzMath [45,46] - mathematical library.

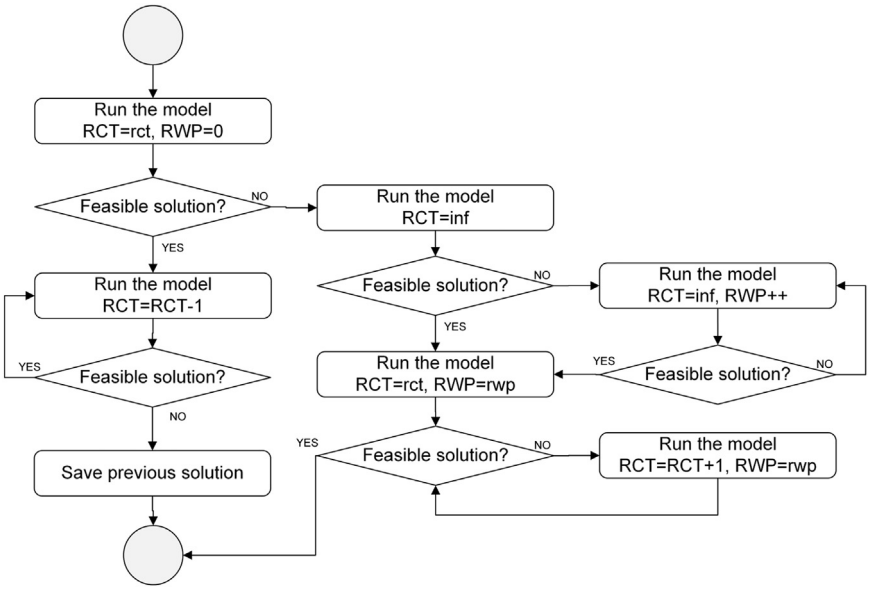


**Fig. 8.** Algorithm for the obtainment of a feasible solution for the linear mixed-integer model – Stage 3.

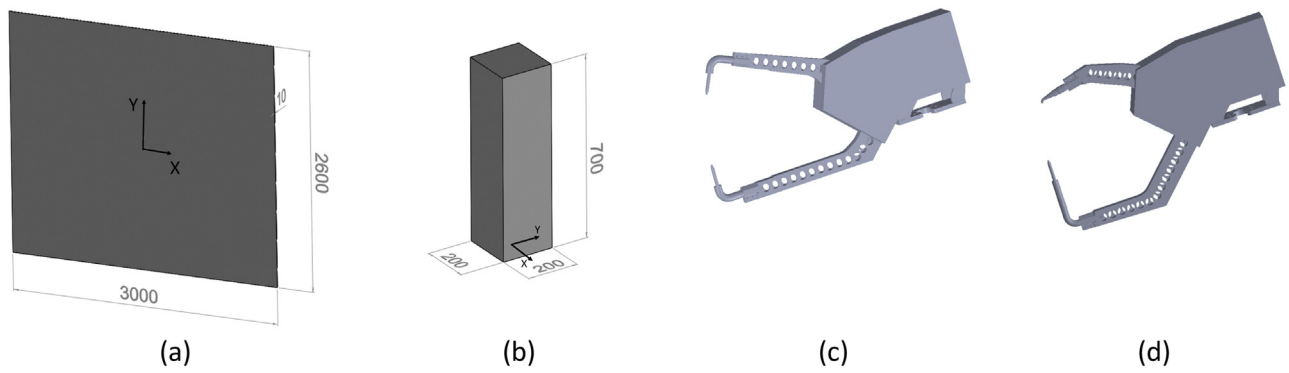


**Fig. 9.** Simplified case – cell resources.

## 5. Application scenario

The proposed approach has been tested on:

- a sets of 7 generated simplified cases (Section 5.1)
- 1 industrial case (Section 5.2)

The sets of generated cases is strongly connected to real problems even if characterized by simplified environment. The cases have been implemented to assess the quality of the approach proposed in this paper. The computational time is analyzed in Section 5.3.

### 5.1. Simplified cases

Seven simplified cases have been generated and analyzed. These cases, standardized in order to be replicated and useful in order to calibrate the approach, differ in the positions of the twelve considered welding points. These welding points are randomly selected in 3 circle area having as center the points presented in Table 19 and an increasing radius (from 50 mm of the first case to 650 mm of the last case with a step of 100 mm). The rotation (*aer* Euler convention) is predefined for each point. The center points are placed in front of the 3 possible considered *RPOs* (Fig. 10, Fig. 11 and Table 16).

The elements considered for the cell design are:

- metal sheets *BIW* (Fig. 9a) placed in as described in Table 14.
- 18 fixturing element *BF* (Fig. 9b) placed as described in Table 15.
- COMAU Smart NH4-200-2.7.
- ground robot support structure.
- Two welding gun models *WGMs* (Fig. 9c and d) mounted as described in Fig. 17 and Table 17. The robot in $RPO_1$ can mount both the welding guns, while the robot in remaining position can only mount $WGM_1$.

The required cycle time (RCT) is 25 s (Figs. 10 and 11). The costs of the resources are presented in Table 5. For sake of brevity, only the simplified case 1 is reported hereafter. All the remaining cases are presented in Appendix B (Tables 20–31).

#### 5.1.1. Simplified case 1

Simplified case 1 aims to solve the cell design and motion planning for the *WPs* in Table 19 . The radius of the circles for the generation of the *WPs* is 50 mm.

The final solution is characterized by the selection of all the 3 robots (Fig. 12, Table 6). The welding gun model $WGM_2$ is allocated to the robot in $RPO_1$, since it presents the same accessibility to the welding points but it is cheaper. $RPO_1$ is responsible for the welding of $WP_1$, $WP_2$, $WP_3$ and $WP_4$; $RPO_2$ is responsible for the welding of $WP_7$; $RPO_3$ is responsible for the welding of $WP_5$, $WP_6$, $WP_8$, $WP_9$, $WP_{10}$, $WP_{11}$ and $WP_{12}$. The cell cycle time, due to the robot in $RPO_3$, is equal to 23.2 s, thus coping with the *RCT*. Finally, the cell cost is equal to 328,500€. From the robot selection point of view, this cost is minimized since the minimum number of necessary robots is found (the allocation of $WP_7$ to the robot in $RPO_2$ is necessary in order to cope with the *RCT*). From the welding gun point of view, $WGM_2$ is selected for the robot in $RPO_1$ since it presents the same reachability of the $WGM_1$ with a minor cost.

#### 5.1.2. Considerations

All the seven cases were successfully solved, coping with the requested cycle time. The provided solutions differ in terms of number of robots and selected welding guns. All the simplified cases required 3 robots, except for the simplified case 2 that

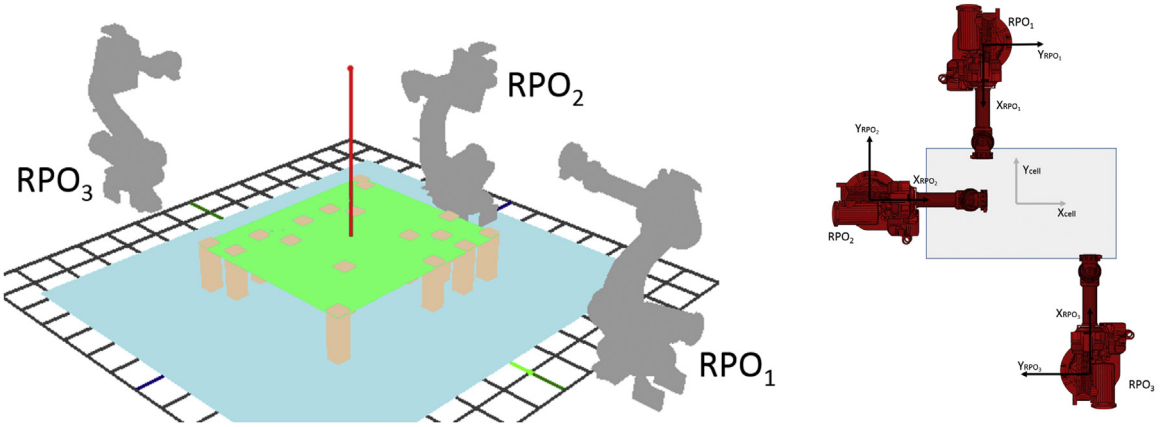


**Fig. 10.** Simplified case – possible RPOs in the cell environment.

required 2 robots (Table 21). As expected, the highest time was presented by the simplified case 2 (the case with the lowest number of robots).

### 5.2. Industrial case

The considered industrial case was provided by COMAU S.p. A., FCA group. The cell is composed by 3 robots SMART-NH4-200-2.7 mounted on the ground, 3 welding gun models (Fig. 13), a fixturing system composed by 35 elements. 3 possible *RPOs* were considered. The first robot (in $RPO_1$) mounts the $WGM_1$ and welds 7 points. The second robot (in $RPO_2$) mounts the welding gun $WGM_2$ and it is responsible for 8 welding points. The third robot (in $RPO_3$) mounts the $WGM_3$ and welds 7 points. The cell cycle time is 40 s. $WGM_1$, $WGM_2$ and $WGM_3$ present a different spatial occupancy and costs and grant a different accessibility. The input data are in Table 7, Table 32, Table 8. The resource costs were modified in comparison to the real costs for confidentiality issues. In order to test the developed approach in the industrial case (Fig. 14), an alternative orientation for the robot in $RPO_1$ is introduced, defining the new robot position/orientation $RPO_4$ ($-45$ degrees around robot Z axis). Moreover, the possibility to mount the $WGM_3$ on robot in $RPO_2$ is analyzed. Table 7–9 and Table 20 resume the input data related to welding guns and robot positions/orientations.

The case was successfully solved (Fig. 15). The solution is characterized by a cost of 272270€ determined by the selection of 3 robots in $RPO_2$, $RPO_3$, $RPO_4$ (Table 10) and the allocation of the $WGM_2$ to the robot in $RPO_2$. The cost of the cell resources is minimized. The selection of the $WGM_2$ instead of $WGM_3$ for $RPO_2$ is not driven by the cost, but by the WPs reachability: the selection of $WGM_3$ would have not granted the reachability of 3 welding points, thus preventing the obtainment of a feasible solution.

The results were compared with the concept of the industrial cell, even if they were not implemented in a real cell. The comparison between the obtained cell design and the industrial solution reveals that the robot in $RPO_4$ is preferred to the robot in $RPO_2$. This solution represents an alternative, since the *WP* reachability granted by the robots is the same, none of the trajectories of the two robots collide with the other robot trajectories and the robot cycle time is lower than the cell cycle time. The

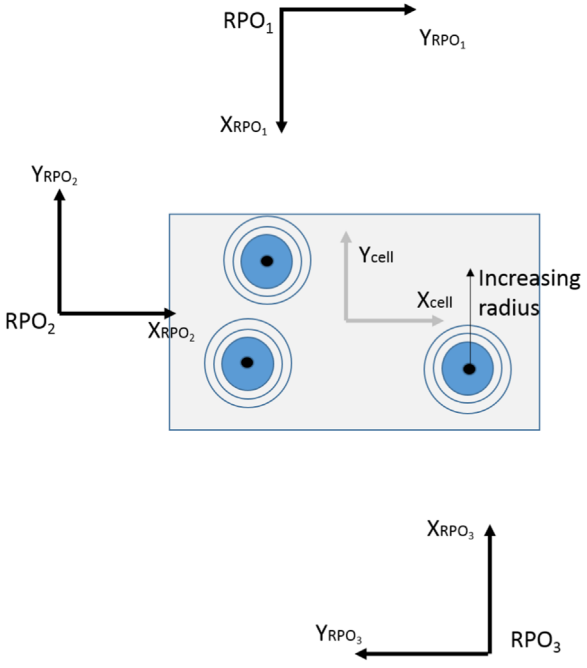


**Fig. 11.** Simplified case – circular areas for WPs sampling.

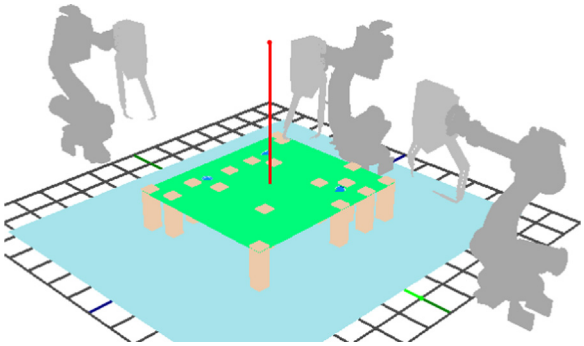

**Fig. 12.** Simplified case 1 – provided solution.

obtained cycle time is 37.2 s, thus 2.8 s lower than the cycle time declared by the company (40 s). The allocation of the *WPs* to the robot is equal to the allocation of the industrial solution, even if the welding sequences are different. Robot in $RPO_2$ and $RPO_3$ start simultaneously, while robot in $RPO_4$ starts 8 s after. Robot in $RPO_3$ and $RPO_4$ end respectively at 20.88 s and 36.32 s. Thus, the cell cycle time depends on the robot in $RPO_2$. The Stage 1 algorithms and criteria required the sampling of 3000 Halton points and obstacles-based 500 points. The nearest-$n$ algorithms was used with $n = 100$. The linear trajectory research was employed for the connection of $WP_8$ and $WP_{12}$. The defined trajectories do not show unnecessary movements of the robot (Fig. 16).

### 5.3. Computational time

The time required for the resolution of the presented cases on a 2.66 GHz processor laptop are depicted in Table 11. On the one hand, the ad-hoc cases require a reduced computational time for Stage 1 resolution coherently with the lower complexity of the environment. On the other hand, the time required in Stage 3 by the industrial case is inherently lower due to a minor number of combinations to be analyzed (the number of robots that can reach the same welding point is limited).

## 6. Conclusions and future work

Design and motion planning of multi-robot spot welding cells are labor intensive and time-consuming activities, generally managed in a manual way by specialized worker and different functional units. This work proposes an approach aiming at simultaneously and automatically solving the two problems, thus leading to the reduction of the required time and human effort.

The proposed approach consists of four stages, granting the simultaneous cell design and coordinated robot motion plan. The *motion planning* approach is based on an off-line decoupled motion planning techniques for high-dimensional $\mathcal{C}$-spaces and articulated robots in order to grant applicability to multi-robot cell for spot welding. The motion plan for each single robot is defined through existing techniques (Stage 1), whereas the coordination of the robot is based on a new developed model applied to articulated robots (Stage 2 and 3).

The existing techniques adapted for Stage 1 (probabilistic roadmap) were improved to cope with the high complexity of the environment that characterizes multi-robot spot-welding cells. The motion plan is based on the Open Robot Realistic Library that catches the real robot behavior during trajectory generation. OBB hierarchical decomposition is employed for collision checking. *Cell design* is solved simultaneously to multi-robot motion planning in Stage 3. The final provided solution is validated through simulation (Stage 4).

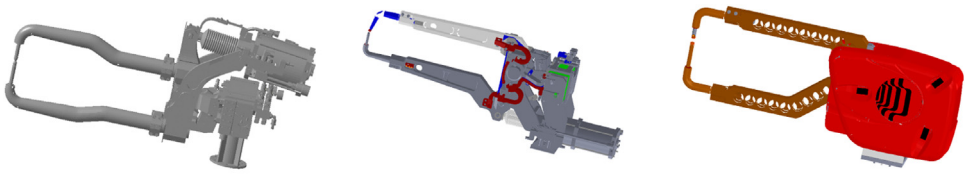

(a) Welding gun 1 (b) Welding gun 2 (c) Welding gun 3

**Fig. 13.** Industrial case – input – welding guns.

The approach was tested on a set of ad-hoc cases and an industrial case provided by the Italian company COMAU S.p. A. The set of ad-hoc cases were correctly solved, showing the approach feasibility. The resolution of the industrial case leads to a successful test bed.

In the following, conclusions both from the scientific and the industrial point of view will be drawn, limitations will be highlighted and future work will be sketched.

### 6.1. Scientific contributions

From a theoretical prospective, the work proposes an extended formalization of design and motion planning problems for spot-welding multi-robot cells. Moreover, the wide number of factors accounted as problem variables is novel. As discussed in Section 2, some papers handle the resolution of the design and motion planning problems for multi-robot spot-welding cells, taking into account the selection of the robot position and orientation and the multi-robot motion planning. On the contrary, this work has considered the following factors: selection of the robot model, selection of the welding gun models, the allocation of the welding gun models to the robots, robot position and orientation, allocation of the welding points to the robots, single-robot motion planning and the multi-robot motion planning.

### 6.2. Industrial advantages

The main advantages deriving from the industrial application of the developed approach consist in:

- The decrease of the time needed for the design and motion planning from some weeks of manual work to some days of simulation and manual work. Manual work will be limited to the preparation of the data and to adjustment of the final solution, if needed.
- Independence of the results from the worker's expertize, which was formalized and integrated into the developed algorithms.

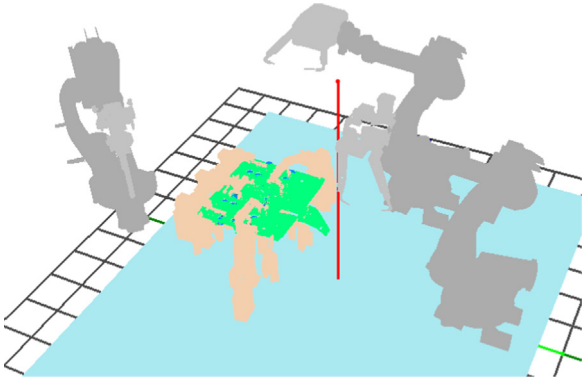

**Fig. 15.** Industrial case – provided solution.

### 6.3. Limitations

The limitations to the developed methodology are:

1. The methodology is currently able to manage one robot model per cell;
2. The possible number of robot position and orientation that can be contemporary analyzed is limited respect to the number of robots that can be employed in the cells;

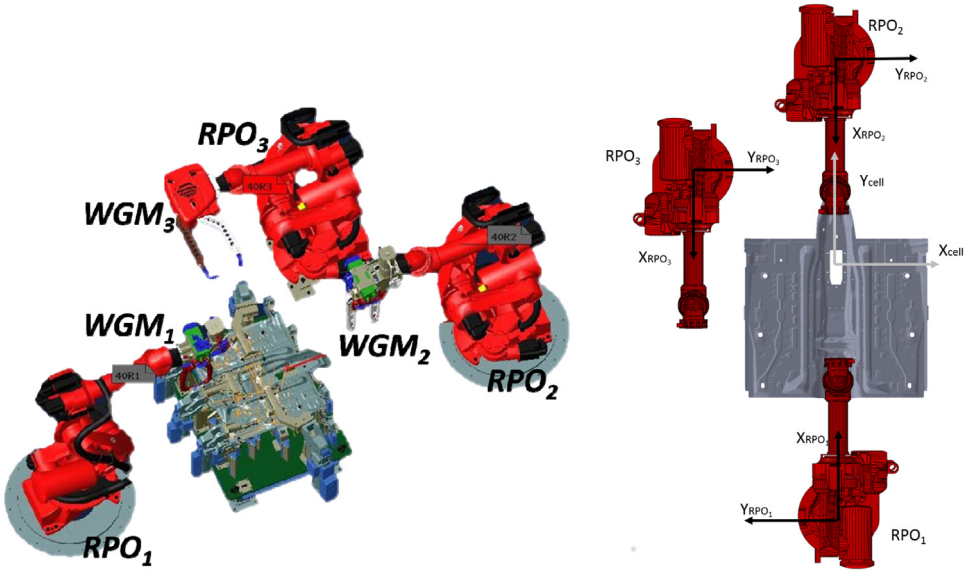


**Fig. 14.** Industrial case – input – cell design.

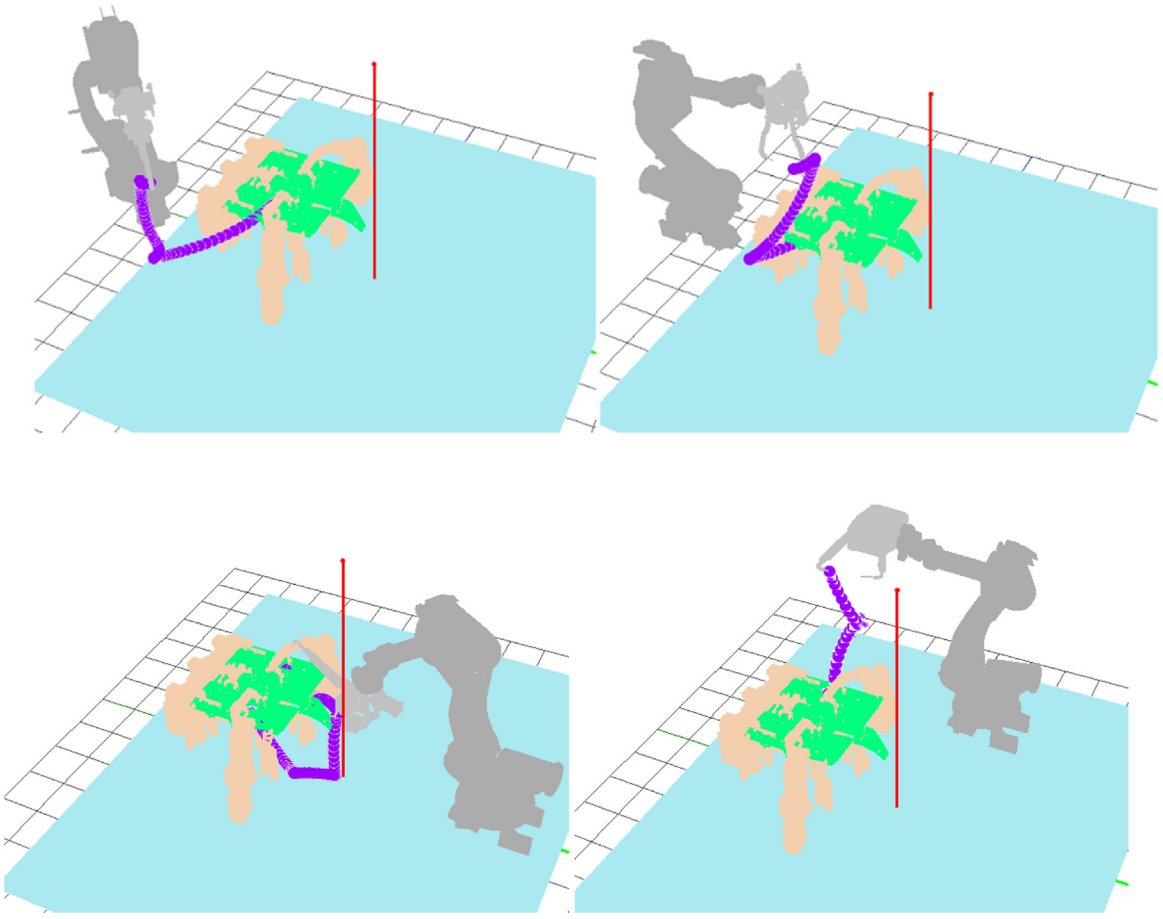

**Fig. 16.** Industrial case – examples of generated path.

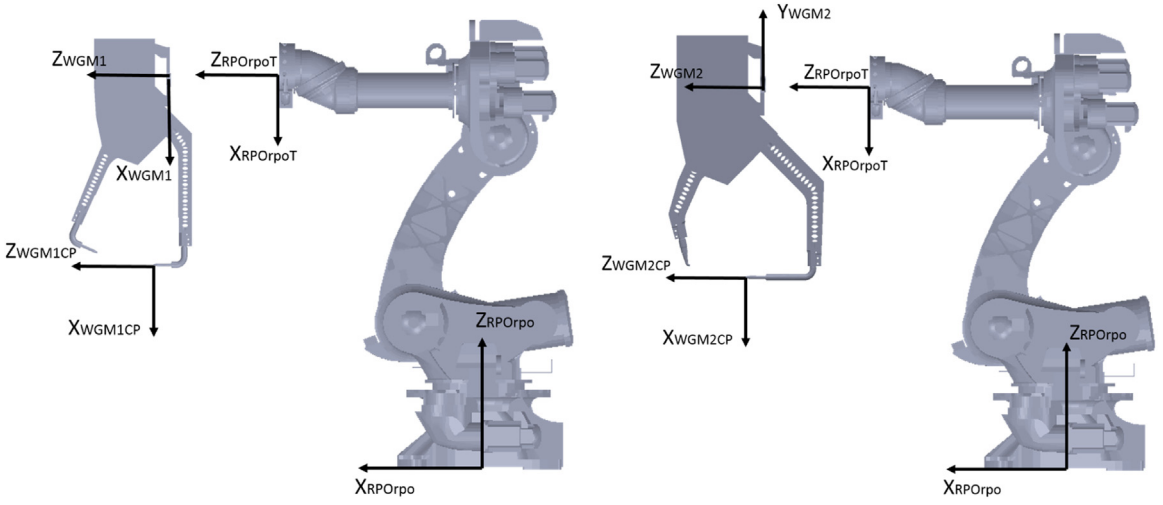


**Fig. 17.** Simplified case – welding gun model reference systems.

3. The methodology provides a solution for around 20 points. Spot welding cells with hundreds of welding points cannot be currently managed by this approach;
4. Precedence constraints among the welding points were not included in Stage 3 in order to reduce the computational complexity of the model. However, this was not a problem in the resolution of the industrial case in which precedence constraints do not exist.
5. If the methodology is not able to provide a solution coping with the required cell cycle time due to robot coordination difficulties, the solution with the lowest cell cycle will be provided;
6. Due to the use of the ORL, the approach can only consider COMAU robots.

A possible way to overcome these limitations is presented in the next section.

**Table 32**
Industrial case – welding points (expressed w.r.t. the cell reference frame, linear unit [mm], rotational unit [deg]).

| $WP_{wp}$ | x | y | z | a | e | r | Flag | $WT_{wp}$ |
|---|---|---|---|---|---|---|---|---|
| $WP_1$ | 181 | −1109.7 | 1048.04 | 90 | 2.636 | 82.615 | W | 1.1 |
| $WP_2$ | 586.5 | −1112.21 | 1049.35 | 90 | 2.636 | 54.769 | W | 1.1 |
| $WP_3$ | 420.75 | −1112.21 | 1049.35 | 90 | 2.636 | 74.885 | W | 1.1 |
| $WP_4$ | 320.84 | −1290.79 | 1057.58 | 90 | 2.636 | 98.182 | W | 1.1 |
| $WP_5$ | 612.19 | −1290.82 | 1047.23 | -175.08 | 0 | 0 | W | 1.1 |
| $WP_6$ | 182.03 | −1353.13 | 1057.84 | 90 | 2.636 | 74.51 | W | 1.1 |
| $WP_7$ | 325.44 | −1414.65 | 1063.28 | 90 | 2.636 | 82.683 | W | 1.1 |
| $WP_8$ | −586.5 | −942.01 | 1041.52 | 90 | 2.636 | −179.175 | | 1.1 |
| $WP_9$ | 586.5 | −942.01 | 1041.52 | 90 | 2.636 | 179.175 | | 1.1 |
| $WP_{10}$ | −419.31 | −942.01 | 1041.52 | 90 | 2.636 | 167.358 | | 1.1 |
| $WP_{11}$ | 419.31 | −942.01 | 1041.52 | 90 | 2.636 | −167.358 | | 1.1 |
| $WP_{12}$ | -181 | −945.91 | 1039.5 | 90 | 2.636 | −172.245 | | 1.1 |
| $WP_{13}$ | 181 | −945.91 | 1039.5 | 90 | 2.636 | 172.245 | | 1.1 |
| $WP_{14}$ | −100.88 | −1017.34 | 962.04 | −179.412 | 110.98 | 87.21 | | 1.1 |
| $WP_{15}$ | 100.88 | −1017.34 | 962.04 | −0.58 | 110.98 | −85.21 | W T4:1 | 1.1 |
| $WP_{16}$ | −181 | −1109.7 | 1048.04 | 90 | 2.63 | −86.54 | | 1.1 |
| $WP_{17}$ | −586.5 | −1112.21 | 1049.35 | 90 | 2.63 | −80.54 | | 1.1 |
| $WP_{18}$ | −420.12 | −1112.21 | 1049.35 | 90 | 2.63 | −82.54 | | 1.1 |
| $WP_{19}$ | −320.84 | −1290.79 | 1057.58 | 90 | 2.63 | −101.764 | | 1.1 |
| $WP_{20}$ | −612.19 | −1290.82 | 1047.23 | -26.87 | 0 | 0 | | 1.1 |
| $WP_{21}$ | −182.06 | −1353.06 | 1059.24 | 90 | 2.63 | −75.23 | | 1.1 |
| $WP_{22}$ | −325.44 | −1414.65 | 1063.28 | 90 | 2.63 | −83.23 | | 1.1 |

### 6.4. Future work

Future work will concern, on the one hand, the overtaking of the existent limitations and, on the other hand, the general extension of the approach.

*First direction* – in order to cope with the limitations described above, Stage 3 could be revised. Indeed, Stage 3 is responsible for (i) the restriction in the number of analyzable welding points, robot models and robot positions/orientations (limitations 1, 2 and 3) and (ii) the absence of precedence constraints (limitation 4). Specifically, the restriction to the number of problem inputs and in considering precedence constraints is due to the already high computational complexity of the mixed integer mathematical model of Stage 3. A significant increase in the number of inputs or the introduction of precedence constraints may lead to an overflow during the model resolution. A possible solution could be based on the simplification of the model through its decomposition and the cyclical resolution of the identified sub-problems until a solution is found.
*Second direction* – as explained in Section 4.3, the possible fault in robot coordination (limitation 5) could be avoided through the modification of the hypothesis at the basis of the definition of safe and unsafe couples of trajectories. Several research directions could be addressed. For instance, the model could be changed introducing a level of safety for each couple of trajectories, thus allowing a partial temporal overlapping during the trajectory execution according to the identified level.
*Third direction* – the limitation related to the applicability of the methodology to cells involving COMAU robots (limitation 6) could be easily overtaken by the use of the realistic robot simulation – RRS – the world-wide de-facto standard for precise simulation of robot motion behavior.

## Acknowledgments

The research has been partially funded by the Italian 'Industria 2015 - Mobilitá Sostenibile' project 'FlexProd: Sistemi di Produzione Flessibili ed Eco-Efficienti per Veicoli su Gomma' (i.e., Flexible and Eco-sustainable Systems for the production of vehicles). The authors want to thank COMAU S.p. A. for its strong commitment in this research, for the sharing of its knowledge in spot-welding processes and for the several industrial provided cases.

## Appendix A. – inputs and outputs in the approach stages

See Tables 12,13.

## Appendix B. – test case data

### B.1. Simplified cases

See Tables 14–31, Fig. 17.

### B.2. Industrial case

See Table 32.

## References

[1] S.J. Hu, J. Ko, L. Weyand, H.A. ElMaraghy, T.K. Lien, Y. Koren, et al., Assembly system design and operations for product variety, CIRP Ann. Manuf. Technol. 60 (2011) 715–733.
[2] G. Putnik, A. Sluga, H. ElMaraghy, R. Teti, Y. Koren, T. Tolio, et al., Scalability in manufacturing systems design and operation: State-of-the-art and future developments roadmap, CIRP Ann. Manuf. Technol. 62 (2013) 751–774.
[3] Z.J. Pasek, Customization and automotive industry: in search for new modalities, in: Proceedings of the 2007 World Conf. Mass Cust. Pers., Cambridge, MA, 2007.
[4] Z.J. Pasek, A. Al-Zaher, Towards Reconfigurable Body Framing Systems for Automotive Manufacturing, in: Proceedings of Emerg. Technol. Fact. Autom. (ETFA), 2010 IEEE Conf., Bilbao, 2010, pp. 1–4.
[5] Statista. The statistics portal, 2015. ⟨www.statista.com⟩, Visited on March 2015.
[6] W. Dong, H. Li, X. Teng, Off-line programming of Spot-weld Robot for Car-body in White Based on Robcad, in: Proceedings of IEEE Int. Conf. Mechatronics Autom., Harbin, China, 2007.
[7] M. Sarkans, L. Roosimolder, Implementation of robot welding cells using

modular approach, Estonian J. Eng. 16 (2010) 317–327.
[8] M. Sarkans, L. Roosimolder, Welding robot cell implementation in SME-S using modular approach – case study, in: Proceedings of the 7th Int. DAAAM Balt. Conf. 'in Ind. Eng., Tallinn, Estonia, 2010.
[9] A. Watanabe, Y. Nagatsuka, T. Kosaka, Robot off-line simulation apparatus, US Pat. 7,512,459, 2004, ⟨http://www.google.com/patents/US7512459⟩ (accessed 02.09.14).
[10] R.V. Rao, B.K. Patel, Industrial robot selection using a novel decision making method considering objective and subjective preferences, Robot. Auton. Syst. 59 (2011) 367–375, http://dx.doi.org/10.1016/j.robot.2011.01.005.
[11] R. Kumar, Optimal selection of robots by using distance based approach method, Robot. Comput. Integr. Manuf. 26 (2010) 500–506, http://dx.doi.org/10.1016/j.rcim.2010.03.012.
[12] G. Michalos, S. Makris, N. Papakostas, D. Mourtzis, G. Chryssolouris, Automotive assembly technologies review: challenges and outlook for a flexible and adaptive approach, CIRP J. Manuf. Sci. Technol. 2 (2010) 81–91.
[13] A. Al-Zaher, W. ElMaraghy, Z.J. Pasek, Enabling car body customization through automotive framing systems design, in: Hoda ElMaraghy (Ed.), Enabling Manuf. Compet. Econ. Sustain., Springer Berlin Heidelberg, 2012, pp. 445–451.
[14] A. Al-Zaher, W. ElMaraghy, Z.J. Pasek, RMS design methodology for automotive framing systems BIW, J. Manuf. Syst. 32 (2013) 436–448.
[15] A. Al-Zaher, W. ElMaraghy, Cost-effective Design of Automotive Framing Systems Using Flexibility and Reconfigurability Principles, University of Windsor, 2013.
[16] A. Al-Zaher, W. ElMaraghy, Design of reconfigurable automotive framing system, CIRP Ann. Manuf. Technol. 62 (2013) 491–494.
[17] H. Choset, K.M. Lynch, S. Hutchinson, G. Kantor, W. Burgard, L.E. Kavraki, et al., Principles of Robot Motion, The MIT Press, London, England, 2005.
[18] K. Kant, S.W. Zucker, Toward efficient trajectory planning: the path-velocity decomposition, J. Int. J. Robot. Res. 5 (1986) 72–89.
[19] J. Peng, S. Akella, Coordinating multiple robots with kinodynamic constraints along specified paths, Int. J. Robot. Res. 24 (2005) 295–310.
[20] S.S. Chiddarwar, N.R. Babu, Conflict free coordinated path planning for multiple robots using a dynamic path modification sequence, J. Robot. Auton. Syst. 59 (2011) 508–518.
[21] P. Svestka, M. Overmars, Coordinated path planning for multiple robots, Robot. Auton. Syst. 23 (1998) 125–152.
[22] G. Sanchez, J.-C. Latombe, On delaying collision checking in PRM planning: application to multi-robot coordination, Int. J. Robot. Res. 21 (2002) 5–26.
[23] G. Sanchez, J.-C. Latombe, Using RPM planner to compare centralized and decoupled planning for multi-robot systems, in: Proceedings of IEEE Int. Conf. Robot. Autom., Washington D.C., 2002.
[24] U. Rossgoderer, C. Woenckhaus, A concept for automatical layout generation, in: Proceedings of IEEE Int. Conf. Robot. Autom., 1995, pp. 800–805.
[25] F.L. Hammond, K. Shimada, Improvement of Manufacturing Workcell Layout Design Using Weighted Isotropy Metrics, in: Proceedings of IEEE Int. Conf. Mechatronics Autom., Changchun, China, 2009, pp. 3408–3414.
[26] Y. Huang, L.B. Gueta, R. Chiba, T. Arai, T. Ueyama, M. Sug, et al., Manipulator system selection based on evaluation of task completion time and cost, in: Proceedings of IEEE/RSJ Int. Conf. Intell. Robot. Syst. Syst., 2011, pp. 25–30.
[27] N. Papakostas, K. Alexopoulos, A. Kopanakis, Integrating digital manufacturing and simulation tools in the assembly design process: a cooperating robots cell case, CIRP J. Manuf. Sci. Technol. 4 (2011) 96–100.
[28] N. Papakostas, G. Michalos, S. Makris, D. Zouzias, G. Chryssolouris, Industrial applications with cooperating robots for the flexible assembly, Int. J. Comput. Integr. Manuf. 24 (2011) 650–660.
[29] CimStation, AC&E, ⟨http://www.acel.co.uk/cimstation-robotics/⟩, last visited: April 2016.
[30] RobCad, Siemens, ⟨https://www.plm.automation.siemens.com/en_us/products/tecnomatix /manufacturing-simulation/robotics/robcad.shtml⟩, last visited: April 2016.
[31] RobotStudio, ABB Robotics, ⟨http://new.abb.com/products/robotics/robotstudio⟩, last visited: April 2016.
[32] 3DAutomate, Visual Components, ⟨http://www.visualcomponents.com/products/3dautomate⟩, last visited: April 2016.
[33] Delmia, Dassault Systems, ⟨http://www.3ds.com/products-services/delmia⟩, last visited: April 2016.
[34] Industrial Path Planner, ⟨http://www.fcc.chalmers.se/software/ips⟩, last visited: April 2016.
[35] COMAU S.p.A., ORL - COMAU web page, ⟨http://www.comau.com⟩, last visited: April 2016.
[36] R. Geraerts, M. Overmars, A comparative study of probabilistic roadmap planners, in: J.-D., B. Boissonnat Joel, Ken Goldberg, Seth Hutchinson (Eds.), Algorithmic Found. Robot. V, Springer, Berlin Heidelberg, 2004, pp. 43–58.
[37] R. Geraerts, M.H. Overmars, Sampling Techniques for Probabilistic Roadmap Planners, Institute of information and computing sciences, Utrecht University, 2003.
[38] R. Dechter, J. Pearl, Generalized best-first search strategies and the optimality of A*, J. ACM (1985), http://dx.doi.org/10.1145/3828.3830.
[39] S. Gottschalk, M.C. Lin, D. Manocha, OBBTree: A Hierarchical Structure for Rapid Interference Detection, in: SIGGRAPH '96 Proceedings of the 23rd Annu. Conf. Comput. Graph. Interact. Tech., 1996, pp. 171–180.
[40] R. Geraerts, Sampling-based Motion Planning: Analysis and Path Quality, PhD Dissertation, Netherland, 2006.
[41] M. Peternell, H. Pottmann, T. Steiner, H. Zhao, Swept volumes, Comput. Des. Appl 2 (2005) 599–608.
[42] T. Tolio, Design of Flexible Production Systems, Springer, Milano, Italy 2009 http://dx.doi.org/10.1007/978-3-540-85414-2.
[43] OpenGL, ⟨https://www.opengl.org/⟩, last visited: June 2016.
[44] Cplex, IBM ILOG CPLEX V12.1, ⟨http://www-03.ibm.com/software/products/en/ ibmilogcpleoptistud⟩, last visited: June 2016.
[45] G. Buzzi-Ferraris, BzzMath: Numerical Libraries in C++, Politecnico di Milano, ⟨www.chem.polimi.it/homes/gbuzzi⟩, (last visited: June 2016).
[46] G. Buzzi-Ferraris, F. Manenti, BzzMath: library overview and recent advances in numerical methods, Comput. Aided Chem. Eng. 30 (2) (2012) 1312–1316.